ELSEVIER

Biochimica et Biophysica Acta 1561 (2001) 1–25

BIOCHIMICA ET BIOPHYSICA ACTA

BBA

www.bba-direct.com

Review

Flexoelectricity of model and living membranes

Alexander G. Petrov *

Institute of Solid State Physics, Bulgarian Academy of Sciences, 72 Tzarigradsko chaussee, 1784 Sofia, Bulgaria

Received 25 April 2001; received in revised form 14 June 2001; accepted 20 June 2001

Abstract

The theory and experiments on model and biomembrane flexoelectricity are reviewed. Biological implications of flexoelectricity are underlined. Molecular machinery and molecular electronics applications are pointed out.

Keywords: Bilayer lipid membrane; Biomembrane; Curvature; Flexoelectricity; Mechanosensitivity; Electromotility; Membrane machine; Molecular electronics

1. Introduction

In 1943 Erwin Schrödinger postulated that a living cell should function like a mechanism [1]. He was then concerned about 'solid' parts of the cells, i.e. DNA molecules.

The present review aims at an extension of Schrödinger's postulate to the liquid crystal parts of the cell, the biomembranes. In the first place this implies the recognition of the existence of an appropriate mechanical degree of freedom in a biomembrane. Furthermore, the recognition of some specific, mechanical pathways for energy transformation in biomembranes is needed.

Biomembranes constitute the basic building units of the majority of cells and cellular organelles. It appears that most membranes are built up according to the general principles of lyotropic liquid crystal structures [2]. The widely accepted 'fluid lipid–globular protein mosaic model' [3–5] claims that lipids are organized in a bilayer in which the proteins are immersed. Model membranes containing lipids only,

Abbreviations: AFM, atomic force microscopy; BLM, black lipid membrane; DPhPC, diphytanoylphosphatidylcholine; EYPC, egg yolk phosphatidylcholine; GMO, glyceryl monooleate; LC, liquid crystal; PC, phosphatidylcholine (lecithin); PE, phosphatidylethanolamine; PS, phosphatidylserine; pp, peak-to-peak; rms, root mean square; UA, uranyl acetate; A, area per molecule; c_0, spontaneous curvature; $c_{1,2}$, principal curvatures; d, membrane thickness; E, electric field; e, proton charge; f, flexoelectric coefficient; H, field coupling parameter; I_f, flexoelectric current; I_ω, first harmonic current amplitude; $I_{2\omega}$, second harmonic current amplitude ; K, curvature elastic modulus of a bilayer; k_B, Boltzmann constant; N, number of molecules per unit area; P_S, electric polarization per unit area; p, hydrostatic pressure difference; T, absolute temperature; t, curvature elastic torque; U, voltage difference; U_f, flexoelectric voltage; ΔV, surface potential, interfacial potential difference; β, degree of dissociation of polar head; δ_N, neutral monolayer surface distance to the bilayer's mid-surface; δ_H, head's surface distance to the neutral monolayer's surface; ε_L, dielectric constant of lipid core of bilayer; ε_w, dielectric constant of water; ε_0, absolute dielectric permittivity of free space; η, viscosity; λ_D, Debye length; μ, electric dipole moment; ν, frequency; σ, surface charge density; σ_a, surface tension; χ, dielectric susceptibility; ψ_d, dipole surface potential; ψ_0, charge surface potential; ω, angular frequency

* Fax: +359-2-975-36-32. *E-mail address:* director@issp.bas.bg (A.G. Petrov).

0005-2736/01/$ – see front matter
PII: S0304-4157(01)00007-7

or lipids with just one type of protein, etc., are also well known.

A membrane has a number of mechanical degrees of freedom: area stretching, thickness compression, shear deformation, chain tilting, and, notably, curvature deformation. The last one, curvature, is just a liquid crystal degree of freedom since membrane curvature is equivalent to a splay of lipid chains (under the condition that chains remain parallel to the local normal in each point of the curved bilayer).

The first striking impression when looking at an electron micrograph of a cell is that cell membranes very often tend to be strongly curved. Unlike tensile or compressive strain, it is very easy to sustain curvature strains (torques) in a membrane because of the smallness of its curvature elastic modulus K [6] (typically a few k_BT units). Examples include the highly convoluted cristae of inner mitochondrial membranes in energized mitochondria, the edges of retinal rod outer segments and discs, the tylakoid membranes of chloroplasts, the brush borders of intestinal epithelial cells, the spiculae tips in echynocytes, the microvilli between contacting cells, the stereocilia in the hearing organ, etc. In many cases this curvature is dynamic, e.g. there is good evidence that the peripheral protein network of a red blood cell membrane is able to produce a membrane curvature at its contraction.

2. Membrane curvature and flexoelectricity

Flexoelectricity is a mechanoelectric phenomenon known from liquid crystal physics. In the case of a membrane flexoelectricity stands for curvature-induced membrane polarization [10,7]:

$$P_S = f(c_1 + c_2) \tag{1}$$

where P_S is the electric polarization per unit area in C/m, c_1 and c_2 are the two principal radii of membrane curvature in m^{-1} and f is the area flexoelectric coefficient in C (coulombs), typically a few units of electron charge (Fig. 1). This effect is manifested in liquid crystalline membrane structures where an overall curvature is related to an orientational deformation of the splay type of membrane molecules (lipids, proteins) (cf. [8]). Across a polarized membrane a potential difference develops according to

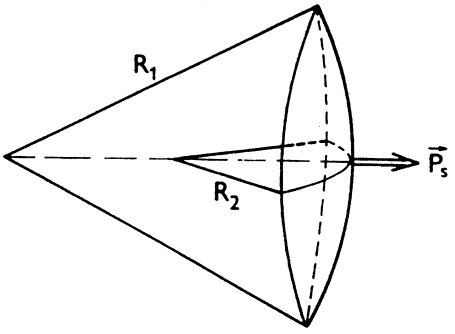

Fig. 1. Flexoelectric (curvature-induced) polarization P_S and sign convention about flexocoefficient f: for the case shown f will be positive. R_1 and R_2 are principal radii of membrane curvature (from [7], with permission from the publisher).

the Helmholtz equation. Its curvature-dependent part reads:

$$\Delta U = P_S/\varepsilon_0 = (f/\varepsilon_0)(c_1 + c_2) \tag{2}$$

By measuring simultaneously this potential difference and the curvature, one can determine a flexoelectric coefficient of a given membrane. Like the piezoelectric effect in solid crystals, the flexoelectric one can also be manifested as a direct effect (Eq. 1) and a converse effect, featuring electric field-induced curvature [7]:

$$c_1 + c_2 = (f/K)E \tag{3}$$

where E is the transmembrane electric field (strictly speaking, an averaged field according to Eq. 10 below) and K is the curvature elastic modulus. Eq. 3 is valid for a tension-free membrane (identically zero lateral tension), which is the case in an osmotically balanced cell.

Following [9] phenomenological equations of membrane flexoelectricity can be written in terms of first derivatives of a thermodynamic potential of a flexoelectric body with curvature deformation and electric field as independent variables:

$$t = \frac{\partial H_E}{\partial c_+} = Kc_+ - f^C E \tag{4a}$$

$$P_s = \frac{\partial H_E}{\partial E} = f^D c_+ + \chi_s E \tag{4b}$$

where H_E (c_+, E) is a thermodynamic potential called electric enthalpy, $c_+ = c_1 + c_2$ is total membrane curvature, χ_s is area dielectric susceptibility ($= \chi d$),

$$f^{\mathrm{D}} = \frac{\partial^2 H_E}{\partial c_+ \partial E} \text{ is direct flexocoefficient,}$$

$$f^{\mathrm{C}} = \frac{\partial^2 H_E}{\partial E \partial c_+} \text{ is converse flexocoefficient.} \qquad (5)$$

However, both flexocoefficients must be equal because second derivatives are independent of the sequence of differentiation (Maxwell relation). Therefore, Eqs. 2 and 3 are written in terms of one and the same flexocoefficient f. Eq. 3 follows from Eq. 4a in the case of vanishing curvature elastic torque ($t=0$), while Eq. 1 follows from Eq. 4b when $E=0$.

Exploring the molecular mechanisms of flexoelectricity is a central task of the liquid crystal approach in membranology [11,12,7]. The flexoelectric coefficient can be represented as an integral over the derivative of $P_z(z)$, the distribution of the normal component of polarization across the membrane (see below). Model distributions including electric monopoles, dipoles and quadrupoles of lipids and proteins have been considered [7], revealing respective contributions to f.

3. Flexoelectricity of membranes and polarization distribution

A basic object in the theory is the distribution of polarization along membrane normal, $P(z,c_+)$.

If it is known, then flexocoefficients can be expressed as integrals of its curvature derivative, as follows.

3.1. Direct flexocoefficient

Area polarization is expressed as:

$$P_{\mathrm{S}} = \int P(z,c_+)dz = \int \left[P^0(z) + \frac{\partial P}{\partial c_+}|_0\, c_+\right] dz =$$

$$P_{\mathrm{S}}^0 + \left[\int \frac{\partial P(z,c_+)}{\partial c_+}|_0\, dz\right] c_+ \qquad (6)$$

i.e. direct flexocoefficient is given by:

$$f^{\mathrm{D}} = \int \frac{\partial P(z,c_+)}{\partial c_+}|_0\, dz \qquad (7)$$

that is, by an integral of the curvature derivative of polarization distribution in a flat membrane at zero electric field, over membrane thickness.

3.2. Converse flexocoefficient

Applying an electric field across a *flat* membrane, its electric enthalpy term is given by the product of its preexisting polarization and the applied field:

$$H_E = -\int P(z,c_+)E\, dz$$

From the first phenomenological equation one gets then for the torque (note that $c_+=0$):

$$t = -\frac{\partial}{\partial c_+}\int P(z,c_+)E\, dz = -\overline{E}\int \frac{\partial P}{\partial c_+}|_0\, dz \qquad (8)$$

i.e. converse flexocoefficient is:

$$f^{\mathrm{C}} = \int \frac{\partial P(z,c_+)}{\partial c_+}|_0\, dz \qquad (9)$$

This proves the validity of the Maxwell relation for a membrane, and demonstrates that both direct and converse flexocoefficients depend on the polarization distribution across a *flat* membrane and at *zero* electric field (there is no applied field at the direct flexoeffect calculation).

Moreover, Eq. 8 provides a definition for the average electric field to be used in Eqs. 3, 4a and 4b: the averaging uses the curvature derivative of the polarization as a weighting function:

$$\overline{E} = \frac{\int E(z)\frac{\partial P(z,c_+)}{\partial c_+}|_0\, dz}{\int \frac{\partial P(z,c_+)}{\partial c_+}|_0\, dz} \qquad (10)$$

4. Polarization distribution in lipid bilayers

A molecular theory of flexoelectricity can be developed using the polarization distribution across membrane thickness $P_z(z)$ [13]. An approach based on charge distribution $\rho(z)$ also exists [14]. Since $P_z(z)$ can be expressed as $z\rho(z)$, the two approaches are physically identical. Fig. 2 represents an attempt to combine various theoretical data about polarization

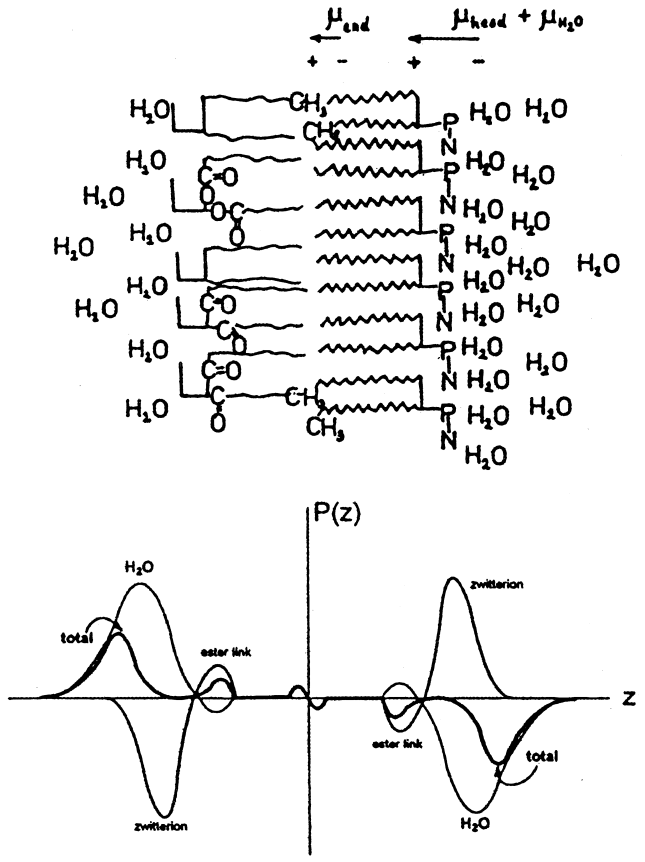

Fig. 2. Schematic distribution of total polarization $P(z)$ (heavy line) across a planar, symmetric, zwitterionic phospholipid bilayer and its two components, lipid polarization (medium line) and water polarization (light line). The peaks indicated would be additionally smeared if small displacements of lipids in a normal direction and chain interdigitations were allowed. μ_{end} is the end CH_3 group dipole. $\mu_{head} + \mu_{H_2O}$ is the resultant dipole moment of head group plus water hydration shell (μ_{head} could further be split into two antiparallel components: $\mu_{zwitter} + \mu_{ester}$) (from [7], with permission from the publisher).

distribution across a flat, symmetric bilayer of zwitterionic phospholipid (lecithin, ethanolamine, etc.).

A major source of polarization comes from the charges distributed over polar head group atoms. Monte Carlo data about z components of dipole moments of lecithin and ethanolamine zwitterions are summarized: both feature a μ_z component of about 14×10^{-30} C.m pointing towards water [15]. On the other hand, according to X-ray data on crystalline lecithin [16], one of the ester links between acid residues and the glycerol backbone (that of the *sn*-2 chain) features a carbonyl dipole pointing towards the bilayer core, i.e. with the positive end inside the membrane, while the other (that of the *sn*-1 chain) is nearly in the plane of the bilayer. The total normal component of the dipole of the carbonyl groups is estimated to be about -3.3×10^{-30} C.m in vacuum [17,18]. Finally, a small dipole, approx. -0.3×10^{-30} C.m, is located at the end of each alkyl chain due to a partial positive charging of the terminal $-CH_3$ [19]. End dipoles of the monolayers should be mutually compensated in a bilayer due to end chain interdigitation.

Adding water to the system makes the computational task rather complicated. However, up-to-date molecular dynamic simulations deal with very realistic molecular structures, including full atomic details of head groups and hydrogen bonding with water [20–25]. These studies reliably elucidate water ordering, head group and hydrocarbon chain conformations and ordering, density profiles, polarization distribution, susceptibility distribution, electrostatic potential profile, etc. For example, probability distribution profiles of water for lecithin and ethanolamine-based bilayers reveal a water penetration up to the region of carbonyl groups, somewhat deeper in the lecithin case due to the larger area per molecule. On the other hand, the orientational polarization profile of water in the lecithin case shows two maxima, with opposite signs, in the region of phosphate and carbonyl groups, and an exponential decay from the choline group towards bulk water. The decay length for the lecithin case is 0.235 ± 0.025 nm and the polarization extends out from the monolayer surface for about 0.7 nm [23]. The polarization curve for ethanolamine shows spike-like features in the region of phosphate and carbonyl groups due to water penetration. These water molecules are highly ordered because of hydrogen bonding. The profile for lecithin is smoother compared to ethanolamine, probably due to more water penetration in the interface region caused by a larger lipid–lipid spacing. The decay length of water polarization in the ethanolamine case is about 0.175 nm [23].

Other simulations clearly demonstrate that the zwitterion dipoles of lecithin are actually overcompensated by hydration water, while carbonyl dipoles are partially compensated [25]. The susceptibility profile suggests a dielectric constant around 30 for the head group–water interface and a dielectric con-

stant around 10 for the ester group region. The potential difference between membrane interior and the aqueous solution, or the membrane dipole potential, is 600 mV, with the main contribution from the carbonyl groups of 450 mV and overcompensation from oriented water of 150 mV [25]. The ester groups' contribution seems exaggerated, though, as the dipole potential difference between ester and ether lecithins (lacking carbonyl groups) is experimentally only about 120 mV [26]. Almost complete compensation everywhere across the head group region (ester region included) is reported in the MD simulation of DPPC [20]. Therefore, oriented water in the immediate bilayer vicinity probably makes a major, non-compensated contribution.

These considerations lead us to the conclusion that interfacial water, being orientationally ordered and polarized, should be regarded as an integral part of liquid crystal bilayers and membranes as soon as their flexoelectricity is concerned.

The discussion above considered purely dipolar lipids. However, even zwitterions carry an exactly zero net charge of the polar head at a specific pH value only, i.e. at their isoelectric point. A number of other biologically important lipids (phosphatidylserine, phosphatidic acid, etc.) are charged even at neutral pH, this charge being negative in most cases. In that case the charge asymmetry gives rise to another source of polarization, the electric double layer polarization of the surface charges on membrane interfaces with the diffuse double layers of their counterions. For our purposes this polarization component is sufficiently well described by the classical Debye–Hückel theory (e.g. [27]).

No matter what the actual distribution of polarization across a lipid bilayer looks like, it is obvious that in a flat, symmetric bilayer $P_z(z,c)$ will be an antisymmetric function about the mid-plane (Fig. 2). For a curved bilayer this is no longer valid. We shall consider below several mechanisms, destroying the antisymmetry of $P_z(z)$ and leading to a non-zero P_S in curved bilayers. In general, all electric multipoles, i.e. charge, dipole and quadrupole, are expected to contribute to the total flexocoefficient:

$$f = f^{C} + f^{D} + f^{Q} \tag{11}$$

the relative amounts of the contributions being dependent on the molecular structure of lipids and the ionic conditions of the bathing electrolyte. If a bilayer is asymmetric in the flat state, then flexoelectricity will add a curvature-dependent component to its total polarization.

5. Dipole mechanism of flexoelectricity and molecular dynamics

In the curvature elasticity theory of lipid bilayers a distinction is made between connected and unconnected bilayers [7]. The term 'connected bilayer' refers to the case in which restrictions along the edges or boundaries or internal restrictions do not allow for the monolayers constituting the bilayer to slide freely one over another. The term 'unconnected bilayer' refers to free monolayers that slide freely upon each other at bending according to their relative area changes with no boundary restrictions. We have established an equivalence between the elastic behaviour of a connected bilayer and a bilayer with both lateral and transbilayer lipid diffusion being blocked, while the case when any of these blocks is lifted is equivalent to the behaviour of an unconnected bilayer [7]. Here we shall also consider these two cases separately.

5.1. Dipolar flexoelectricity of connected bilayers: blocked lipid exchange

In a symmetric connected bilayer the neutral surface coincides with the mid-surface, therefore the outer monolayer (o) is expanded while the inner (i) is compressed as a whole (Fig. 3). The change of lipid packing to more loose in the outer monolayer and to more compact in the inner one will lead to conformational changes in the head groups and, most notably, in the structure of the polarized interfacial water. As a result, the normal components of the dipole moments per head in the two monolayers (μ^{o},μ^{i}) will change, in opposite directions at that. Simultaneously, the area density of the dipoles over the two interfaces will change as well. In this way a dipole imbalance with respect to the mid-surface will arise and the symmetric bilayer will become polarized, with a flexocoefficient [7]:

$$f^{DB} = \left(\frac{\mu_0}{A_0} - \frac{d\mu}{dA}\,|_{A_0}\right) d \tag{12}$$

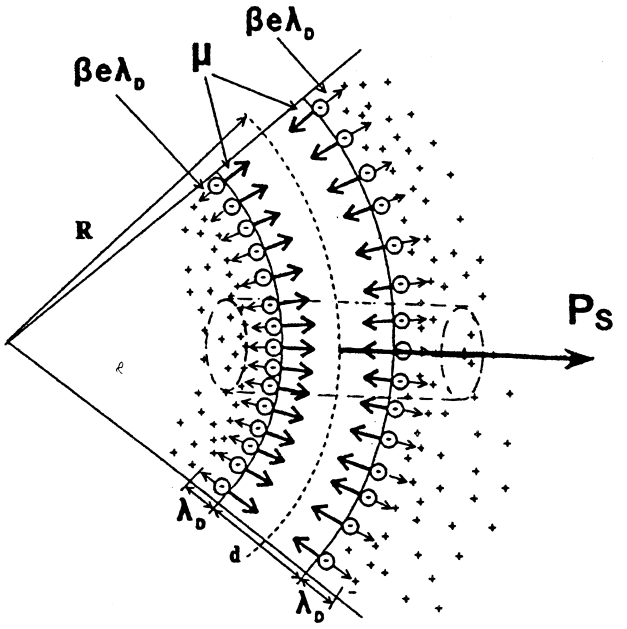

Fig. 3. Flexoelectric polarization P_S of a curved bilayer membrane under blocked lipid exchange. Lipids carry a negative partial charge, β_e, and a permanent dipole moment, μ. Debye length of the diffuse electric double layer is λ_D, $\beta e \lambda_D$ represents the dipole moment (per lipid) of the double layer and d is the membrane thickness (modified from [65], with permission from the author).

where μ is the total normal component of dipole moment per lipid head (polarized water including) and A is the area per lipid head. The superscript DB means the dipolar blocked contribution and the subscript 0 refers to the corresponding values in the flat membrane state. All values in Eq. 15 could be inferred from measurements of the surface potential in lipid monolayers. For asymmetric bilayers the sum of two corresponding expressions of the type of Eq. 12 for each of the monolayers holds.

5.2. *Dipolar flexoelectricity of unconnected bilayers: free lipid exchange*

Unconnected bilayer bending proceeds in such a way that each monolayer is bent around its own neutral surface; relative slippage of the two monolayers is taking place, so that both neutral surfaces remain unstretched and the area per lipid there equals A_0, the area over the mid-surface in the flat bilayer state (Fig. 4). If the distance from the monolayer's neutral surface to the head groups' surface is δ_H, a residual stretching/compression will take place in the region of bilayer interfaces, numerically equal to the stretching/compression of a thinner bilayer, of thickness $2\delta_H$. Consequently, the unconnected flexocoefficient of a symmetric bilayer is immediately obtainable from Eq. 12:

$$f^{DF} = \left(\frac{\mu_0}{A_0} - \frac{d\mu}{dA}\,|_{A_0}\right) 2\delta_H \tag{13}$$

Having established [7] the equivalence between free lipid exchange (either lateral or transversal) and unconnected bilayer bending we can now claim that f^{DF} as given by Eq. 13 represents the free lipid exchange contribution as well.

For a bulk elastic model $\delta_H = d/4$, i.e. $f^{DF} = f^{DB}/2$. If, on the other hand, chain elasticity is vanishing, the neutral surface would coincide with the surface of dipoles, i.e. $\delta_H = 0$ and $f^{DF} \equiv 0$. In any case, the free dipolar contribution is less than the blocked one.

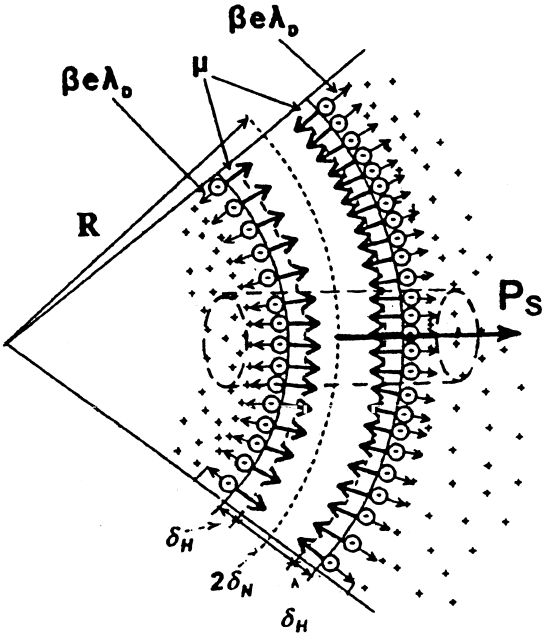

Fig. 4. Flexoelectric polarization P_S of a curved bilayer membrane under free lipid exchange. δ_N is the distance between the neutral and mid-surface, δ_H is the distance between the neutral and the head group surface (modified from [65] with permission from the author). Note that P_S is reduced as compared to the blocked case (Fig. 3) (modified from [65], with permission from the author).

5.3. Flexoelectric polarization and transmembrane voltage difference: estimations of dipole contribution

Applying the Helmholtz equation to a membrane with total area surface polarization P_S (i.e. the sum of permanent plus induced dipoles), we obtain Eq. 2. This expression is strictly valid for a constant P_S over the whole membrane surface, i.e. for a homogeneous total curvature (e.g. spherical or cylindrical curvature). In the case of a position-dependent curvature U_f can be calculated (by dividing the membrane surface S into n fragments of area ΔS with homogeneous curvature) as the average voltage of all these fragments in parallel:

$$U_f = \frac{1}{\varepsilon_0}\frac{\sum_{k=1}^{n}(P_S)_k}{n} = \frac{1}{\varepsilon_0}\frac{\sum_{k=1}^{n}(P_S)_k \Delta S}{S} \underset{\Delta S \to 0}{\longrightarrow} \frac{f}{\varepsilon_0}\frac{\int_S (c_1 + c_2)dS}{S}$$

i.e. the flexovoltage between the two conductive electrolyte solutions separated by an inhomogeneously curved membrane is a non-local quantity governed by the averaged membrane curvature:

$$U_f = \frac{f}{\varepsilon_0}\overline{(c_1 + c_2)} \tag{14}$$

Some authors [28,14] tend to regard Eq. 2 as a definition of a membrane flexocoefficient. However, since U_f (cf. Eq. 14) is a non-local quantity while P_S is local, such a definition is inherently limited to the case of homogeneous curvature. Moreover, it is not applicable to the converse flexoeffect, as U_f could not be a generalized coordinate and generalized force simultaneously (cf. Eqs. 4a and 4b).

Eq. 12 can be rearranged as:

$$f^{DB} = -\varepsilon_0 A_0 d\frac{d(\Delta V)}{dA}|_{A_0} \tag{15}$$

where $\Delta V = \mu/\varepsilon_0 A$ is the surface potential for a lipid monolayer. The corresponding expression with $2\delta_H$ instead of d holds for free lipid exchange.

Eq. 15 can be used to estimate f^D. From [29] for a DPPC monolayer it follows that $f^{DB} = 1.2 \times 10^{-20}$ C. Correspondingly, f^{DF} will be about 2 times lower. From another set of data for DPPC [30] we obtain $f^{DB} = 1.4 \times 10^{-20}$ C, in good agreement with the previous estimate. A slightly higher value for f^{DB} is obtained for diphytanoylphosphatidylcholine (DPhPC) [31]: $f^{DB} = 1.7 \times 10^{-20}$ C. From the same work it can be inferred that adsorption of PEG on DPhPC monolayers or introduction of PEG-grafted lipids in the monolayer leads to the appearance of extended ranges with an opposite sign of the surface potential derivative: $d(\Delta V)/dA > 0$. This means, according to Eq. 15, that PEG-lipids can reverse the sign of the dipolar flexocoefficient from positive to negative.

6. Monopole mechanisms of flexoelectricity

If the lipid molecules comprising a black lipid membrane (BLM) are electrically charged (with partial charge per head βe), two separate situations may be considered leading to different flexoelectric coefficients.

6.1. Detailed electric neutrality

If, after curving, each membrane side remains electrically neutral (surface charge being neutralized by the diffuse layer of counterions) the situation is qualitatively identical to the dipolar lipid model described above. In the low surface potential limit corresponding charge flexoelectric coefficients are easily obtainable from Eqs. 15 and 16 by replacing the permanent dipole moment, μ, with the effective dipole moment of the diffuse electric double layer $\mu_D = \beta e \lambda_D/\varepsilon_w$ (cf. Figs. 3 and 4). λ_D, the Debye screening length, gives an effective distance from the charged lipid heads to the diffuse layer of counterions.

Let us consider now the degree of ionization, β, as area dependent, $\beta(A)$. Possible reasons for a non-zero derivative, $d\beta/dA$, could be variations of the adsorption/desorption of counterions and a shift of the proton equilibrium over the membrane surfaces due to the change of the available area and/or packing-induced changes of the polar head conformation. Such conformational changes will, in turn, change the accessibility of the charged groups for protons and counterions. With respect to protons, this could be

expressed in terms of a curvature-induced shift of the surface pK_a values of the ionizable groups over the membrane surface. Bearing in mind that double layer dipoles are centred at a distance $\lambda_D/2$ away from the membrane surface (Fig. 3), we obtain for a blocked lipid exchange

$$f^{CB} = \frac{e}{\varepsilon_w}\left(\frac{\beta_0}{A_0} - \frac{d\beta}{dA}|_{A_0}\right)\lambda_D(d+\lambda_D) \quad (16)$$

and, consequently, for a free lipid exchange (Fig. 4):

$$f^{CF} = \frac{e}{\varepsilon_w}\left(\frac{\beta_0}{A_0} - \frac{d\beta}{dA}|_{A_0}\right)\lambda_D(2\delta_H+\lambda_D) \quad (17)$$

where subscript 0 refers to the flat membrane state.

Note that f^{DB} and f^{DF} in Eqs. 12 and 13 have positive signs if μ points towards the non-polar membrane core (the usual case found in lipid monolayers by surface potential measurements) and that f^{CB} and f^{CF} in Eqs. 16 and 17 bear the sign of β (i.e. the sign of the surface charge). Therefore, for negatively charged lipids (the usual case with biologically relevant lipid molecules), both contributions to f (f^D and f^C) have different signs and tend to reduce each other (Figs. 3 and 4). Since λ_D is one order of magnitude larger than the length of the permanent dipoles (approx. 1 nm at 0.1 M ionic strength), the charge contribution would be expected to be larger than the dipolar one. However, double layer dipoles are situated in a highly polar medium that is accounted for here by $\varepsilon_w \approx 30$. Therefore, the two contributions are of the same order of magnitude [14]. In fact, surface potential measurements even demonstrate that a permanent dipole contribution prevails at a lower degree of ionization [32,29].

Eq. 15 permits us also to relate the sum of f^C+f^D to surface potential variations. If, instead of μ we take $\mu+\mu_D$, then Eq. 15 will hold again, this time with $\Delta V = \psi_d+\psi_0$. Typically, in the range of 70 Å^2, $d\Delta V/dA = -6\times10^{17}$ V/m^2 [29,30,33]. With $d+\lambda_D$ = 6 nm, we then get $f^{CB}+f^{DB} = 2.2\times10^{-20}$C.

Finally, we should note that Eqs. 16 and 17 are strictly valid at low surface potentials, i.e. at low partial charge per head ($\beta[\%] < 5.8/\lambda_D$[nm]), when Grahame and Poisson–Boltzmann equations can be linearized. Direct calculation of the voltage difference across a spherically curved bilayer by solving the linearized Poisson–Boltzmann equation [34] confirms the validity of Eqs. 16 and 17 under the additional requirement $R >> \lambda_D$ that is always fulfilled at high enough ion concentration. The influence of the adsorption/desorption of monovalent and multivalent counterions has also been analysed using the Langmuir adsorption model [34,35].

By solving the non-linear Poisson–Boltzmann equation for charged symmetric bilayers, a self-consistent effective increase of surface charge density of the outer monolayer (and an opposite in sign decrease of the inner one) was obtained [36] for a cylindrically curved bilayer (of curvature radius R) as follows (assuming that the surfaces of charges are neutral surfaces for each of the monolayers):

$$\Delta\sigma = \frac{2k_BT}{e}\varepsilon_w\frac{(q-1)}{p}\frac{H}{q+H}\frac{1}{R} \quad (18)$$

where

$$p = \frac{\sigma e\lambda_D}{2\varepsilon_w k_B T},$$

$$q = \sqrt{1+p^2}$$

and

$$H = \frac{\varepsilon_L}{\varepsilon_w}\frac{2\lambda_D}{d}$$

is the electric coupling parameter. Multiplying these effective charges by the membrane thickness d we shall obtain an expression for the area flexoelectric polarization in the non-linear case. In the limit $p \ll 1$ and with weak electric coupling ($H \ll 1$) the resulting expression for the flexocoefficient ($f = (\varepsilon_L/\varepsilon_w)\sigma\lambda_D^2$) closely resembles Eq. 17 with $\delta_H = 0$ (the surface of the charges is a neutral surface) and $d\beta/dA = 0$, apart from an additional factor of ε_L in the nominator.

6.2. Global electric neutrality

If, by curving the membrane, effective displacement of electric charges across the whole membrane thickness takes place (e.g. an excess of negative charges over the expanded outer surface and deficiency over the compressed inner surface, equivalent to an excess positive charge), this will result in a large electric dipole situated in a low polar medium (ε_L), and, consequently, the curvature-induced voltage dif-

ference will be large. This effect, called a shift of surface charge equilibrium, was discussed in the general case of $\beta \neq 0$, $d\beta/dA \neq 0$ [37], and subsequently considered from a fundamental electrostatic point of view [14] in a special case of an area-independent degree of dissociation ($d\beta/dA = 0$). The results again differ for blocked and free lipid exchange. They are again obtainable from Eqs. 12 and 13, this time by replacing the permanent dipole moment μ with the effective dipole moment of the surface charges with respect to the bilayer's mid-surface: $-\beta e d/2\varepsilon_L$. We shall denote here the corresponding flexoelectric coefficients by f^M (monopole) in order to distinguish them from the case of detailed electric neutrality.

$$f^{MB} = \frac{e}{\varepsilon_L}\left(\frac{\beta_0}{A_0} - \frac{d\beta}{dA}\,|_{A_0}\right)\frac{d^2}{2} \tag{19}$$

$$f^{MF} = \frac{e}{\varepsilon_L}\left(\frac{\beta_0}{A_0} - \frac{d\beta}{dA}\,|_{A_0}\right) d\delta_H \tag{20}$$

Comparing Eqs. 16 and 17 with Eqs. 19 and 20 we see that it holds:

$$f^M = -\frac{d}{2\lambda_D}\frac{\varepsilon_w}{\varepsilon_L} f^C = -\frac{1}{H} f^C \tag{21}$$

Consequently, the flexocoefficients for the two monopole mechanisms differ in sign and, depending on the smallness of the coupling parameter H, the difference in their magnitudes can reach about two orders, i.e. $f^M \approx 1 \times 10^{-18}$ C. This really makes the second mechanism a leading one for the monopole case. Furthermore, estimations from monolayer measurements [37,38] show that $d\beta/dA$ is making the most of the contribution. With $d\beta/dA = -5 \times 10^{18}$ m^{-2}, $d = 5 \times 10^{-9}$ m, $e = 1.6 \times 10^{-19}$ C and $\varepsilon_L = 2$, Eq. 19 yields $f^{MB} = -5 \times 10^{-18}$ C.

Let us also note the fact that most measurements of flexocoefficients (Table 1), in the presence of even a low amount of surface charge, reveal these characteristically higher values. However, the effect of $d\beta/dA$ is clearly predominant since β/A is typically about -2×10^{17} m^{-2} only.

The mechanism of the shift of surface charge equilibrium implies that the excess charges emerging on the two membrane surfaces compensate each other across the membrane thickness, rather than being compensated by the diffuse double-layer counterions [14,37]. Indeed, if these opposite-in-sign excess charges on the two membrane surfaces were distributed continuously, the electric field created by them would be confined within the membrane capacitor. Some leakage field may be expected, though, in the discrete distribution case, leading to some degree of external compensation.

7. Quadrupolar mechanism

Following [7] the area quadrupolar flexocoefficient will be:

$$f^Q = \frac{1}{3} L_{zz} \theta_a d \tag{22}$$

where θ_a is the anisotropy of Θ_{ij}, the quadrupole moment tensor of the molecule, L_{ij} is the Lorentz local field tensor ($L_{ij} > 0$). For lipids we could estimate [39] $f^Q \approx -1 \times 10^{-20}$ C. This is the same order of magnitude as f^D, but the sign is opposite. For membranes containing cholesterol f^Q may be enhanced. It is certainly higher for biomembranes with high protein concentration.

8. Flexoelectricity and membrane proteins

We shall complete the theoretical description of flexoelectricity with some remarks concerning living membranes. The first important feature of biomembranes is the strongly heterogeneous lipid composition of the liquid crystal membrane matrix. Studies of mixed lipid monolayers [40] demonstrate that the variation of dipole moment per molecule as a function of the area differs from those of pure monolayers: depending on the composition, $d\mu/dA$ can be either enhanced or weakened. This may be due to the different sorts of water structure created around different head groups (e.g. lecithin and sphingomyelin) and the lack of correspondence at the overlapping of their hydration shells. Biomembranes are complicated mixtures of various lipids.

Integral proteins could provide a great contribution to the curvature-induced membrane polarization. Both dipolar and quadrupolar contributions could be expected, more pronounced than those of

the lipids. The cause of such an expectation is the very large dipole moment measured for some proteins: 666×10^{-30} C.m for myoglobins, 1666×10^{-30} C.m for haemoglobins [41,42]. Theoretical calculations also demonstrate that such big molecules with no spherical symmetry in charge distribution have very large anisotropy of the quadrupole moment [43].

8.1. Dipole contribution of integral proteins

Dipole contribution is preconditioned by free lateral diffusion of proteins. This is a basic assumption in the fluid-mosaic model of biomembranes [3–5]. Protein flip-flop is highly improbable. Monolayer measurements [40] demonstrate the variations of dipole moment of peripheral proteins at stretching or compression. This implies the possibility of 'bimorph' flexoelectricity of peripheral proteins (an analogue of the piezoelectricity of a bimorph plate), especially if these are symmetrically adsorbed over the two membrane interfaces, as suggested in the Danielli–Davson model.

The important structural parameters of proteins with respect to the dipole mechanism are a dipole moment component parallel to the membrane normal μ_p and a conical steric asymmetry $s_p = \alpha/a$, where α is the conical angle and a is the width of the protein (Fig. 5). The angle α is actually a measure of the average deviation of the boundary lipid chains' orientation from the bilayer normal, due to the protein perturbation. Protein shapes need not be conical as a whole; for example, it was assumed [44] that a cylindrical protein with a hydrophobic pocket may induce a tilt of its boundary lipids. A splay of these lipids may also be induced by a spherical protein, if it is asymmetrically embedded in one monolayer only (Fig. 5). Due to the fast rotational diffusion of proteins around the normal axis, chain splay would be in any case cylindrically averaged, i.e. the total splay will be $s_p = 2\alpha/a$.

If a large number of such proteins, unidirectionally oriented, are grouped together in an immediate contact, the membrane will curve as a whole and its total curvature will be s_p. The maximal protein density is N_m. If the protein concentration N is less than N_m, a relative concentration $n = N/N_m < 1$ can be introduced. In that case spontaneous membrane curvature is proportional to n [45]: $c_0 = s_p n$. Following [7] the resulting flexocoefficient is

$$f^{PD} = \frac{K}{k_B T} s_p \mu_p \bar{n}(1-\bar{n}) \quad (23)$$

With $K = 1\times10^{-19}$ J, $\mu_p = 666\times10^{-30}$ C.m, $s_p = 2\times0.1/5\times10^{-9} = 4\times10^{7}$ m^{-1} and $k_B T = 4\times10^{-21}$ J we obtained $\bar{n} = 0.4$ and $f^{PD} = 1.6\times10^{-19}$ C.

This value is one order of magnitude larger than the dipolar contribution. The sign of the flexocoefficient is determined by the mutual orientation of the dipole and steric asymmetry of a protein: positive at parallel orientation and negative at antiparallel orientation.

Similar treatment could be developed for a mixed lipid membrane containing strongly dipolar and strongly asymmetric lipid species.

8.2. Quadrupole contribution of integral proteins

The quadrupolar contribution is mostly expected in membranes with high protein concentration, where ordered arrays of integral proteins do exist. Examples of this type include the purple membranes of *Halobacterium halobium* [46], the inner mitochondrial membrane [47], etc. The presence in biomembranes of extended domains of tightly packed globular proteins in a double tiered pattern is a basic idea in the structure–function unitization model of bio-

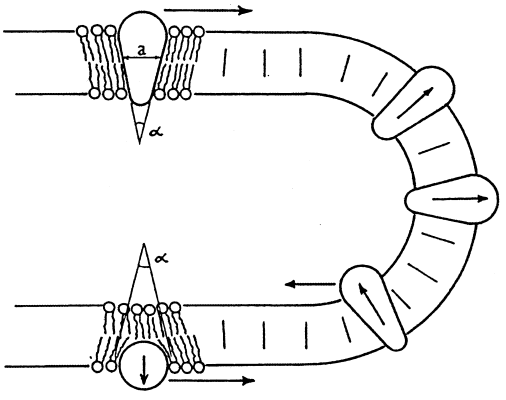

Fig. 5. Flexoelectric dipolar contribution of integral membrane proteins. Asymmetric proteins are laterally redistributed between flat and curved membrane segments. α is the conical angle and a is the width of an asymmetric protein. Favourably oriented proteins are pulled by long range elastic forces in a curved segment while unfavourably oriented proteins are pushed away from it (from [7], with permission from the publisher).

membranes [48]. The flexocoefficient of an array of identical double-tiered quadrupolar proteins will be given by Eq. 22. The anisotropy of the quadrupole moment tensor of membrane proteins has not been measured. It has only theoretically been evaluated to be $\theta_a^M \approx 1.7\times10^{-36}$ C.m^2 for a small soluble protein, carboxypeptidase A [43]. This value could be taken as a lower limit for the larger integral proteins. With a cross-sectional area of a protein macromolecule of the order of 25×10^{-18} m^2, assuming $L_{zz}\approx 1$ we can obtain from Eq. 22: $f^{PQ}\geq 4.5\times10^{-20}$ C as a lower limit. The sign of f^{PQ} depends on the quadrupolar anisotropy of the proteins in the domain. The estimations given above show that the main contribution to the flexoelectric polarization of biomembranes with high protein content would originate from the quadrupolar flexoeffect of integral proteins arranged in double-tiered domains [48]. Bending of such membranes would be rather energy-consuming, though, because of the higher bending stiffness of these structures. Anyway, the well-known fact that the inner mitochondrial membrane is quite smooth in the non-energized state, while in energized mitochondria it is extensively curved [49–52], is quite indicative to us of a possible role for the flexoeffect in the energy transformation. Thus, flexoelectricity could be a missing link in the hypothesis of conformational coupling at the oxidative phosphorylation in mitochondria [53]. Charging of the membrane capacitor could then originate from curvature-induced flexopolarization.

The curving of purple membrane fragments in an external electric field or under surface charge asymmetry [54] could be considered experimental evidence for the existence of a converse quadrupolar flexoeffect of bacteriorhodopsin protein arrays.

9. Experimental studies of flexoelectricity in black lipid membranes and biomembranes

9.1. Theoretical remarks

The first experimental hints about the generation of AC currents by BLMs subjected to oscillating gradients of hydrostatic pressure were obtained accidentally in the early 1970s [55,56]. Subsequently, we noted that pressure-driven currents are much lower and insufficient to explain the experimental data. Furthermore, we stressed upon the variations of membrane curvature in these experiments and explained the effect as a displacement current due to the oscillating flexoelectric polarization of the curved membrane [10–12,57].

Phenomenologically, it is easy to describe this effect in terms of curvature-induced polarization. Using the constitutive Eq. 1, assuming (for simplicity) oscillating spherical curvature and representing it in the form

$$c_1 + c_2 = c(t) = 2c_m \sin \omega t \tag{24}$$

where ω is the angular frequency of oscillations and $c_m = 1/R_m$ is the maximal curvature, we will obtain time-dependent flexopolarization as well. Time-dependent polarization leads to a transmembrane AC voltage difference (Eq. 2) that can be measured in an external circuit of two electrodes immersed in the bathing electrolyte on each side of the membrane, connected to a very high impedance electrometer (open circuit conditions, zero current clamp). The flexoelectric voltage is a first harmonic with respect to curvature oscillation and its amplitude is

$$U_\omega = \frac{f}{\varepsilon_0} 2c_m \tag{25}$$

If, on the other hand, the two electrodes are effectively shorted out via low impedance ammeter (shorted circuit conditions, zero voltage clamp), the displacement current through the meter can be calculated by adopting an equivalent circuit, containing an AC voltage generator U_f (describing the oscillating flexoelectric membrane) and a capacitor C (where C is the membrane capacitance). Since P_S is by definition the total membrane polarization due to both permanent and induced dipoles, the relevant membrane capacitance is simply

$$C_0 = \frac{\varepsilon_0 S_0}{d}$$

where S_0 is the flat membrane area and d is the capacitive thickness of the membrane. Capacitance oscillations will contribute to higher harmonics. Therefore, we have for the first harmonic amplitude of the membrane flexoelectric current

$$I_\omega = f\frac{C_0}{\varepsilon_0} 2c_m \omega \tag{26}$$

In this way, measuring U_ω and c_m, or I_ω, C_0 and c_m, we can determine experimentally the value of the phenomenologically introduced flexocoefficient f. Evaluation of membrane curvature c_m can be performed electrically from the second harmonic of membrane capacitance current under non-zero voltage clamp (the condenser microphone effect) and supposing spherical curvature [37]. Actual curvature (c_1+c_2) can be measured interferometrically [58].

We have seen above that the first three electric multipoles of membrane components (lipids and proteins) contribute to the flexoelectric coefficient. Experimental elucidation of the importance of different multipoles by their independent variation is of substantial interest. Another important subject is the polarization relaxation as it relates to the lipid exchange rate. Such information can be obtained from the frequency dependence of the flexoelectric response.

As we have discussed, lipid exchange can be free or blocked. With blocked exchange, polarization-related processes (head group conformational changes, adsorption/desorption of counterions, proton equilibrium shift) are much faster than the minimum oscillation period of 1 ms used in these studies. Much faster (approx. 1 MHz) also is the relaxation rate of the double electric layer [59]. That relaxation rate governs the establishment of a displacement current in the external circuit. Therefore, we can assume that polarization does indeed follow curvature variations instantaneously. This means that Eqs. 25 and 26 hold for the blocked exchange case, the flexoelectric coefficient f in them being actually f^B. In a BLM, Eqs. 25 and 26 will be effective at higher frequencies when lipid exchange with the bulk phase, the torus, does not proceed fast enough.

In the low frequency limit, $\omega\tau < 1$, where τ is the relaxation time of the lateral exchange, Eq. 25 no longer holds. Time-dependent analysis has been performed [37,35]. The results are:

$$U_f(t) = \frac{1}{\varepsilon_0}\sqrt{\frac{(f^F)^2}{1+\omega^2\tau^2} + \frac{(f^B)^2\omega^2\tau^2}{1+\omega^2\tau^2}}2c_m \sin(\omega t + \phi) = \frac{f(\omega)}{\varepsilon_0}2c_m \sin(\omega t + \phi) \quad (27)$$

$$I_f(t) = \frac{C_0}{\varepsilon_0}\omega\sqrt{\frac{(f^F)^2}{1+\omega^2\tau^2} + \frac{(f^B)^2\omega^2\tau^2}{1+\omega^2\tau^2}}2c_m \sin\left(\omega t + \phi + \frac{\pi}{2}\right) \quad (28)$$

where

$$\tan\phi = \frac{(f^B - f^F)\omega\tau}{f^B\omega^2\tau^2 + f^F}$$

9.2. *Current registration regime: flexoelectric coefficient of bacterial phosphatidylethanolamine (PE) membranes*

First experiments, aimed specifically at registering the flexoelectricity of BLMs from biological lipids (egg yolk phosphatidylcholine (EYPC) [57]; bacterial PE [37]), were performed in the current registration regime using a low impedance current-to-voltage converter. In these experiments the influence of some modifiers of the surface charge and surface dipole, as well as of the membrane conductivity, upon the value of the effect was also studied. BLMs were formed by the classical method of Mueller et al. [60] on a 1 mm conical hole in a Teflon cup, immersed in a spectrophotometric glass cuvette, at room temperature. Bacterial PE (ex. *Escherichia coli*) dissolved in *n*-decane was used as a membrane-forming solution. As a bathing electrolyte either unbuffered KCl (pH 6.2) or buffered KCl with higher or lower pH values was used. The surface charge of the BLM was varied either by pH variation or by adsorption of the ionic detergent cetyltrimethylammonium bromide. The surface dipole was varied by adsorption of the dipole modifier phloretin. Membrane curvature oscillations were excited by the method first employed in [55]: a Teflon cup with a very small internal volume was closed by a Teflon cap. Through an opening in the cap connected to a flexible pneumatic pipeline, oscillating air pressure was applied to the electrolyte surface and transferred in this way to the membrane. Air pressure was generated by an electrically shielded earphone.

Experimentally, the existence of two frequency regions was evident. The median frequency between them was about 150 Hz. In the low frequency region

a slight increase of the signal from 10 to 50 Hz was followed by a plateau up to 120 Hz and by a marked drop of the signal with some membranes around 150 Hz.

In the high frequency region a more or less linear growth of the signal was observed. Extrapolation of the high frequency straight line goes approximately to zero. Qualitatively, the shapes of the characteristics corresponded to the theory (Eq. 28), although the deviations from the straight line in the low frequency range were somewhat stronger and the initial plateau was unexpected.

Phase measurements on pre-curved membranes were performed with the aim of determining the sign of the flexoelectric coefficient in the two frequency regions. Now the membrane oscillated around a curved state and if this static curvature was bigger than the oscillation amplitude, so that the planar state was never reached, the membrane capacitance oscillated with the same (not with the doubled) frequency. Comparing the phases of capacitance current (obtained under non-zero transmembrane voltage) and flexoelectric current (under zero transmembrane voltage), we came to the conclusion that both currents should be in phase when curvature-induced polarization was directed the same way as the transmembrane electric field. For both frequencies this took place when the electric field pointed towards the centre of the membrane curvature. This means that the flexoelectric coefficient was negative in both frequency regions [37].

Such a finding was in accordance with the theoretical prediction for monopole contribution at global electric neutrality (Eqs. 19 and 20), having in mind the leading role of (negative) $d\beta/dA$.

The surface charge of the bacterial PE membrane in the unbuffered electrolyte employed in most measurements (50 mM KCl, pH 6.2) turned out to be negative, with an average value of -1.3 μC/cm^2. Such values, as numerous measurements at this pH showed, were typical for BLMs formed 2–3 days after the preparation of membrane-forming solution (stored in a refrigerator at −4°C). This surface charge density, expressed as $\beta e/A$, corresponded to a partial charge per molecule of $\beta = -5.7\%$ of the proton charge (with mean area per lipid of 0.7 nm^2).

In the high frequency limit (blocked lateral exchange) the flexoelectric coefficient f^B can be calculated from the peak value of the flexoelectric current at a given frequency. We obtained $f^B = -25.5(\pm 72.5\%)\times 10^{-19}$ C for PE/*n*-decane BLM in 50 mM KCl, pH 6.2. Such a high value can only be explained by the charge contribution at global electric neutrality (Eq. 19).

The effect on flexoelectric current of a DPhPC BLM from binding of amphiphilic and lipophilic ions to the membrane was studied recently [61]. The lipophilic tetrakis(*p*-chlorophenyl)borate anion and its fluorophenyl analogue lead to dramatic, one order of magnitude enhancement of flexocurrent. This was readily understood in terms of increased BLM polarizability reflected in a 10 times increased membrane capacitance (cf. Eq. 26). Furthermore, some amphiphilic ions (anions: anthraquinone-2-sulphonate, indole-3-acetate, naphthyl-2-acetate, naphthyl-2-sulphonate; cations: chloroquine, *N*-methyltryptammonium) at asymmetric binding to BLM resulted in a characteristic pattern of substantial dependence of the flexocurrent on the applied transmembrane voltage with a minimum at a certain, ion-specific voltage V_{min}. The sign of V_{min} turned out to be connected to the sign of the ion charge (driving the ion outward the BLM) and the magnitude was determined by the lipophilic group of the amphiphile. This feature may be related to an asymmetric shift and amplification of the BLM tension vs. voltage dependence (Lippmann effect). It provides the opportunity to use flexoelectric membranes as mechanosensors for biphilic ions.

9.3. Voltage registration regime

Further experiments on membrane flexoelectricity were performed in the regime of voltage registration (open external circuit) using a high impedance selective nanovoltmeter. The obtained results provided further evidence of the surface charge contribution in the presence of univalent or divalent ions [62].

BLMs were formed from chromatographically pure lecithin extracted from egg yolk (EYPC). In some experiments mixed BLMs of lecithin with negatively charged phosphatidylserine (PS) were formed. EYPC BLMs modified by uranyl acetate (UA) were prepared by adding different amounts of concentrated UA solution in water to the bathing electrolyte. Strong adsorption of UO_2^{2+} ions on the bilayer

surface was expected, thus resulting in a large positive surface charge depending on the volume concentration of uranyl acetate [63,64]. A two-compartment Teflon chamber (after [56], with some modifications) was used for BLM formation.

Surface charge was estimated by measurements of the electrophoretic mobility of large multilamellar liposomes prepared after Bangham from EYPC in 0.1 M NaCl. Measurements were performed using Mark II (Rank Brothers) electrophoretic equipment. A negative sign of the surface charge was found and a value of $\beta = -0.4\%$ for $A_0 = 0.7$ nm^2 was estimated.

The frequency dependence of the amplitude of the flexoelectric response of pure EYPC membranes showed that above 160 Hz the response was essentially frequency-independent. This is in accordance with Eq. 27 and makes it possible to draw the conclusion that blocked lipid exchange prevails above 160 Hz, quite the same frequency as in the current registration regime. The curve shape from 70 to 160 Hz demonstrated that $f^F > f^B$, as predicted by the theory. The mean value from the measurements from Eq. 21 was $f^B = (26.5 \pm 5.5) \times 10^{-19}$ C for EYPC/*n*-decane BLM in 0.1 M NaCl, pH 6.0. The sign of the flexocoefficient turned out to be positive. The increased flexoresponse from mixed EYPC+2 mol% PS BLMs was demonstrated.

UO_2^{2+}-modified BLMs gave a higher response than unmodified ones for all frequencies. From the plateau values above 300 Hz flexocoefficients f^B in the range of 120–200$\times 10^{-19}$ C were calculated, with a negative sign; the minimum value was at 1 mM UA, the maximum at 3 mM: $f^B = -120 \times 10^{-19}$ ($\pm$ 10%) C for UA-modified EYPC BLM (1 mM UA in 0.1 M NaCl).

Comparing the magnitude of the EYPC flexocoefficient to that of the bacterial PE above we see that they are practically the same, meaning that the surface charge contribution predominates. The difference of signs of the flexocoefficients is more difficult to comprehend in view of the fact that surface charge has the same sign in both cases. The theory does predict a positive sign of f^{DB} (Eq. 12) and f^{CB} (Eq. 16); however, we have seen that these contributions are at least 10 times lower than the f^B magnitudes experimentally found here. On the other hand, the negative sign (and eventually magnitude) of the UA-modified flexocoefficient can be understood on the basis of the reversal and strong enhancement of the surface dipole moment of the tightly adsorbed UO_2^{2+} layer [64].

9.4. Stroboscopic interferometry

Initially, BLM curvatures were evaluated indirectly from the second harmonic capacitance current generated by oscillating BLM clamped at non-zero voltage by assuming, necessarily, completely spherical deformation of an initially flat BLM. A new development was later concentrated on the actual membrane shape under oscillating pressure.

Precise movements of oscillating BLMs have been determined directly by real-time stroboscopic interferometry [58,65,38]. Videorecorded real-time movements of the oscillating BLM interferometric patterns have permitted the precise evaluation of membrane deformation in terms of changes in the radii of curvature along two orthogonal axes, thus obviating the need for assuming completely spherical BLM deformation. Simultaneous electric measurements of U_f led to the first direct determination of the flexoelectric coefficients of glyceryl monooleate (GMO), phosphatidylcholine (PC) and PS BLM in the 100–700 Hz range.

Schematics of the experimental setup used for synchronized electrical and real-time stroboscopic interferometric measurements of BLMs [58] are shown in Fig. 6. This arrangement is analogous to that used in the Mach-Zehnder interferometer, with the exception that mirror 1 was replaced by the BLM (Fig. 6).

In the next stage of these experiments [38] the whole synchronization was put under computer control: the mode-locked frequency of the laser (41.0007 MHz) was fed into the computer and then divided appropriately to the frequency range of membrane oscillations (100–1000 Hz). This new frequency was returned to the laser to serve as the Q-switch and pulse-picking system frequency. On the other hand, the computer fed the function generator, i.e. the transducer, with a slightly different frequency in order to obtain the stroboscopic effect.

The apparent rate of oscillations being slowed by stroboscopy, optical interferograms could be continuously videorecorded at the normal speed of a commercial VHS recorder. A time sequence of images was read from the videotape using a PC-Vision Plus frame-grabber.

Profiles of the BLM were then produced (Fig. 7) and curvatures at extreme BLM positions were calculated, resulting in reliable values of flexoelectric coefficients. Analyses of the errors of this new method were given in [38]. The final error of the flexoelectric coefficient was determined to be 25%. The reproducibility between different BLM preparations was of the same order.

The surface charges of GMO and EYPC BLM were determined by voltage-dependent capacitance measurements under an ionic strength gradient [66,67]. $\sigma = -4.3 \times 10^{-2}$ C/m^2, i.e. $\beta = -18.8\%$ for EYPC (with $A_0 = 0.7$ nm^2) was obtained. However, the same ion gradient caused no shift of capacitance vs. voltage curve minimum away from zero for GMO membranes, demonstrating the complete absence of any surface charge with this dipolar lipid.

Selected interferograms of 300 Hz oscillating curvature changes of a GMO BLM are illustrated in Fig. 7, along with computer-generated profiles of two orthogonal cross-sections, allowing for calculation of principal curvatures. Curvature distribution over the BLM surface may be inhomogeneous, especially at higher frequency [38]. Then, considering the curvature just in the central point often leads to overestimation of overall curvature and thus underestimation of flexocoefficient (cf. Eq. 14). This problem was overcome by combining stroboscopic and capacitance data about curvature [7]. Consequently, the data were re-evaluated: $f^B = (4.3 \pm 0.2) \times 10^{-20}$ C for GMO/*n*-decane BLM in 0.1 M KCl and $f^B = (13.0 \pm 0.3) \times 10^{-19}$ C for EYPC/*n*-decane BLM in 0.1 M KCl. The EYPC value is 30 times higher than that of the GMO, demonstrating the surface charge contribution.

Experimental data on flexoelectric coefficients for bovine brain PS BLMs bathed in aqueous solutions at pH 4.0, 7.0, and 10.0, respectively, as functions of oscillation frequency demonstrated a pH-independent high frequency value of PS flexocoefficient [38]: $f^B = 20(\pm 25\%) \times 10^{-19}$ C for PS/*n*-decane BLM in 0.1 M KCl.

9.5. Converse flexoelectric effect: Maxwell relation

We have seen that both the direct and the converse flexoeffect must exist and, according to the Maxwell relation, both flexoelectric coefficients must be equal.

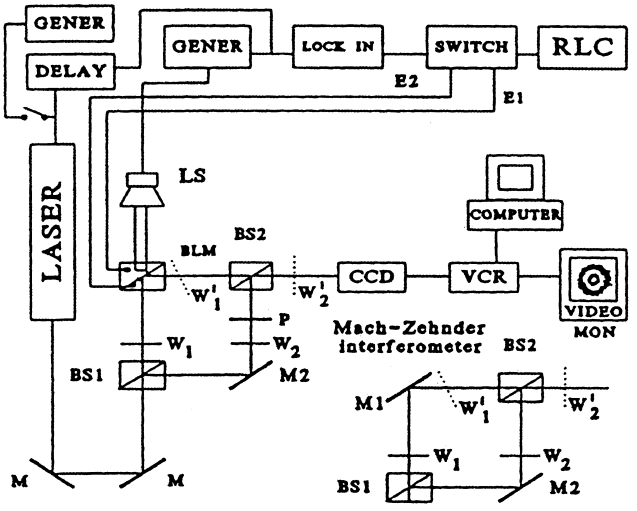

Fig. 6. Schematics of the experimental setup used for simultaneous electrical and real-time stroboscopic interferometric measurements. A Quantronics 4116 Q-switched, mode-locked and pulse-picked Nd:YAG laser provided second harmonic 532 nm, 120 ps, 40 μJ pulses at 50–5000 Hz repetition rate. A Hewlett-Packard 8116 A function generator was used. For static image observation delay was provided by a 111AR Avionics delay generator. Real-time movements of the BLM were observed using a second function generator (Global Specialities) to drive laser pulses. The lock-in was a Dynatrac 391 A Ithaco lock-in amplifier. RLC, 1689 M GENRAD Digibridge; LS, a commercial 8 W loudspeaker; BLM, the cell compartment for the bilayer lipid membrane; BS1 and BS2, beam splitters; M1 and M2, mirrors; CCD, an NEC color camera; VCR, a commercial VHS videorecorder; VIDEO MON, NEC color monitor; COMPUTER, a Hewlett-Packard IBM-compatible PC. For comparison, the scheme of a simple Mach-Zehnder interferometer is included (from [7], with permission from the publisher).

Theoretical analysis showed that lateral tension is a major limiting factor in observing the converse flexoeffect in BLMs. It is important, therefore, to have a BLM able to withstand as high a voltage as possible without rupturing. Therefore, we employed stabilization of bovine brain PS membranes by uranyl acetate.

The experimental setup was similar to the one shown in Fig. 6 except that now curvatures were produced by externally applied transmembrane voltage [68]. Computer-controlled stroboscopic illumination permitted the observation of the motions of the membrane surface in real time by introducing a small frequency difference ($\sim$1 Hz) between the BLM oscillation and the laser pulse frequency. The real-time images were recorded, frame-grabbed and analysed.

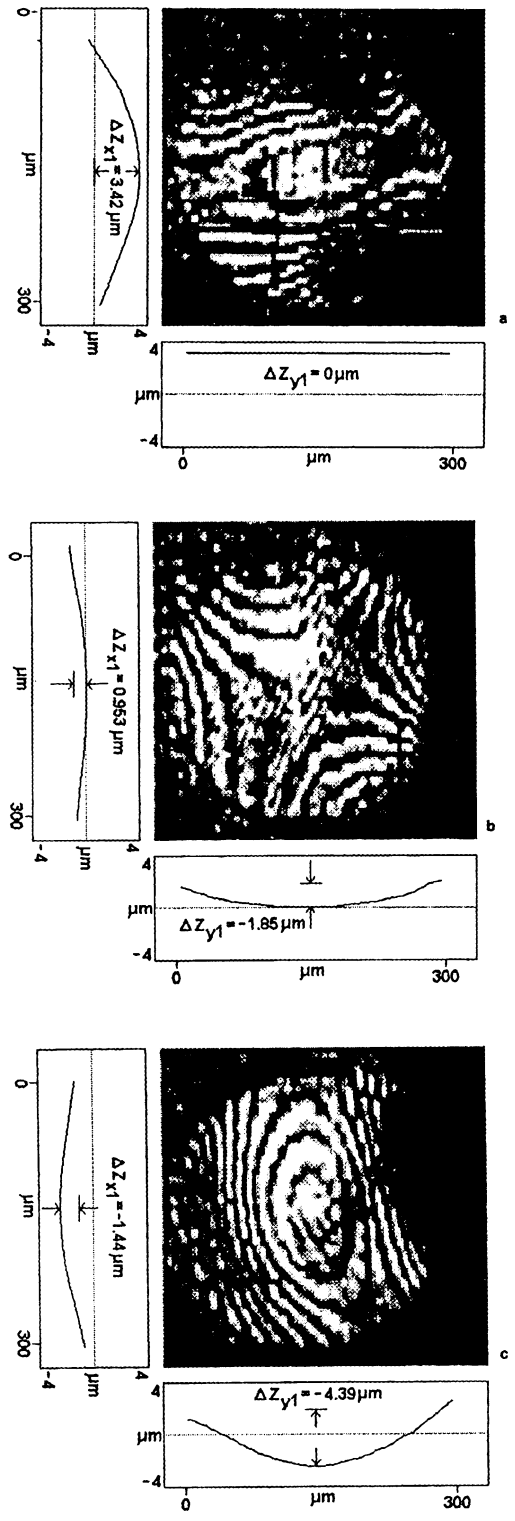

Displacements to the maximum forward and backward excursions of the membrane surface were determined from the captured interferometric images as in the case of direct flexoeffect.

Fig. 7. Typical computer-enhanced interferograms of a GMO BLM at three delay times t. (a) $t = 0$ ms: first extreme position (forward curved). (b) $t = 0.91$ ms: middle position (saddle shaped). (c) $t = 1.67$ ms: second extreme position (backward curved). Notice the difference in scales between x (0–300 μm) and z (−4 to +4 μm) (from [65], with permission from the author).
←

The basic experimental finding was that, under an AC electric potential, curvature oscillations were elicited in the BLM at the same frequency as the applied AC voltage. This was confirmed by our method of stroboscopic interferometry at each of the applied frequencies, from 100 to 450 Hz. The excitation of the fundamental frequency is in accordance with the flexoelectric nature of the effect. A voltage-dependent effect on the BLM tension coupled to some residual pressure differences would have generated a second harmonic (because the tension would have reached two minima within one period of the electric field). This was not the case experimentally.

The frequency dependence of the flexocoefficient values (Fig. 8) reveals two domains: a low frequency one (below 300 Hz) with a lower value of f, and a high frequency one (above 300 Hz) with a higher value of f. Such behaviour is commonly observed in direct flexoeffect as a transition from a regime of free lipid exchange (low frequency) to a regime of blocked lipid exchange (high frequency). The transition frequency varies from one BLM system to another, but is usually in the range of 150–300 Hz. After a low frequency rise, f attains a high frequency plateau value corresponding to f^B. From the fit of the data in Fig. 8 according to the functional dependence $f(\omega)$ in Eq. 27 we obtained [7] $f^B = 151(\pm 19\%) \times 10^{-19}$ C for UA-modified PS BLM (1 mM UA in 0.1 M KCl). This value is in very good agreement with that evaluated earlier by the direct flexoeffect in a (1 mM) UA-modified, egg-lecithin BLM: $120(\pm 10\%) \times 10^{-19}$ C. Egg lecithin had a lower negative surface charge than PS, which was used in the present case. However, once UA^{2+} ion adsorption on the membrane surface was completed (usually at micromolar concentrations), recharging to a high positive surface charge value had taken place [64]. Then, evidently, electric and flexoelectric BLM properties should be dominated by the adsorbed UA ion layer that is known to have a substantial dipole moment [64].

The first observation of the converse flexoeffect in BLMs permits, at least conceptually, the potential use of stabilized BLM systems as microtransducers, micro sound wave generators, and microactuators in molecular electronics. Indeed, flexoelectrically induced displacements of a membrane surface that is only nanometers thick represent (on a molecular scale) a huge, coordinated motion in space of a whole molecular assembly. This effect may, then, find some interesting practical applications.

9.6. *Patch clamp technique and direct flexoeffect of native membranes*

A patch clamp method was originally developed for the investigation of single ion channels. To this aim, small patches of native membranes were sealed at the tips of glass micropipettes. The patch clamp method is well described in the literature [69]. With the development of the tip-dip technique [70,71] formation of model phospholipid membranes on patch clamp pipettes from lipid monolayers also became possible. Thus, the method became available for reconstituted channel studies as well. A novel application of the patch clamp technique is provided by the ability to vary the membrane curvature on a μm scale and, thus, to study the flexoelectric properties of model and native membranes [72–74].

The experimental setup is shown in Fig. 9. Theoretical analysis of the oscillating pressure technique as applied to patch clamp gives for a tension-free patch gives [75]:

$$R = \sqrt[3]{K_S r^2/2p_0} + 8\eta L\nu/3p_0 \qquad (29)$$

After substituting for the elastic modulus $K_S = 50$ mN/m [76], for the tip radius $r = 1$ μm, for the tip length $L = 1$ mm, for the pressure amplitude $p_0 = 1$ torr = 133.3 Pa, for water viscosity $\eta = 1$ cp = 1×10^{-3} J.s/m^3 and for oscillation frequency $\nu = 20$ Hz, Eq. 29 yields: $R = 5.7$ μm+0.4 μm = 6.1 μm.

We see that at 20 Hz the increase of the curvature radius (i.e. the decrease of curvature proper) due to the dissipation of pressure by viscous friction is a minor effect. At 200 Hz the elastic and viscous resistances to patch curving are already comparable for a 1 μm tip radius. Even if K_S tends to zero, viscous friction would prevent the patch curvature from attaining high values; nevertheless, R from Eq. 29 would be comparable to the patch radius. However, if a patch is under tension already in its flat state, then (even neglecting its area elasticity) the Laplace law with an even modest tension of $\sigma_a = 1$ mN/m and a static pressure difference of 1 torr yields $R = 15$ μm. With an oscillating pressure of amplitude p_0 the following solution holds:

$$R = (2\sigma_a + 8\eta L\nu)/p_0 \qquad (30)$$

i.e. the curvature radius will be increased even further. It can be concluded that a tension-free, flaccid patch is essential for the manifestation of substantial oscillating curvature. Tension from the area elasticity also tends to decrease the induced curvature, but to a lesser extent (compare the cubic root dependence on K_S in Eq. 29 to the linear dependence on σ_a in Eq. 30). The effect of patch tension on flexoresponse was demonstrated [72].

This method was first applied to flexoelectric properties of model membrane patches formed by tip-dip technique. Pipettes with large tip openings (up to 10

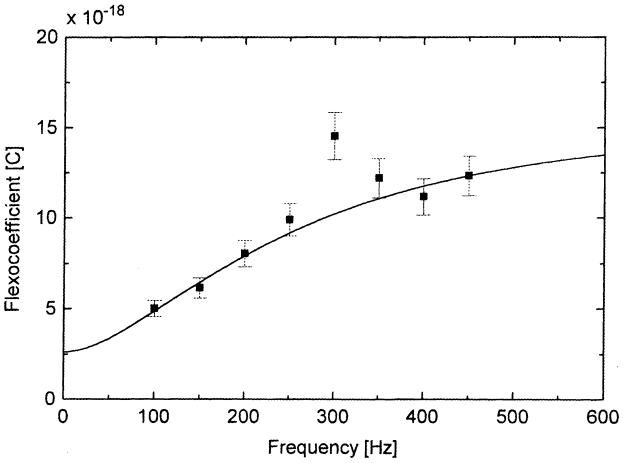

Fig. 8. Converse flexocoefficient of a bovine brain PS (UA^{2+}) BLM vs. oscillation frequency of AC transmembrane potential. Conditions: 25 mg PS in 1 ml *n*-decane at 25°C; BLM modified by 1 mM UA in bathing electrolyte (0.1 M KCl); membrane radius was 143 μm; the amplitude (peak-to-peak) of the applied AC potential was 600 mV. Each point was averaged over at least six successive extreme deviations of the BLM and the relative error in f was typically 9% (after Todorov et al. [38]). The solid line is a fit according to Eq. 8 for $f(\omega)$; fitting parameters are $f^F = (3.0 \pm 1.5) \times 10^{-18}$ C, $f^B = (15.1 \pm 2.9) \times 10^{-18}$ C and $\tau = 440$ ms, i.e. $\nu_m = 362$ Hz (from [7], with permission from the publisher).

μm in diameter) were used. Patches with seal resistance of 0.5–1 GΩ responded more readily to pressure oscillations than those with higher seal resistance. Higher seal resistance means higher adhesion energy of the membrane on the pipette wall and, hence, higher initial tension of the patch σ_a. Over the course of time with some measurements a gradual decay of the response was noticed, which correlated with a gradual rise of seal resistance [72]. Evidently, adhesion energy (and, therefore, patch tension) was slowly increasing with time. Using the approach underlined above, the following flexocoefficient for the synthetic diphytanoyl lecithin was determined [74] in the low frequency range (approx. 20 Hz): $f^F = 0.9(\pm 61\%) \times 10^{-20}$ C for DPhPC patch in 0.15 M KCl, 10 mM BES, pH 7.0.

In another set of experiments in the high frequency range (200 Hz) with the same lipid the result was [78] $f^B = 3.1(\pm 29\%) \times 10^{-20}$ C for DPhPC patch in 0.15 M KCl, unbuffered, pH 6.7. The lower error in the second case was achieved by the consistent use of larger tip diameters, 10–13 μm, instead of 2–5 μm as in the first case.

By adding a charged lipid DPPS, a qualitative increase of flexoresponse was established [74] and subsequently confirmed quantitatively [78]: $f^B = 7.6(\pm 28\%) \times 10^{-20}$ C for DPhPC/DPPS (10:1 mol) patch in 0.15 M KCl, unbuffered, i.e. a 2.4-fold increase of the flexocoefficient.

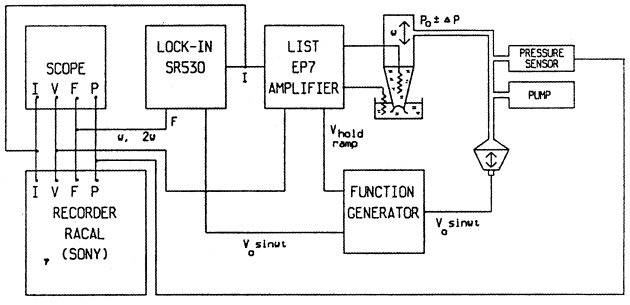

Fig. 9. Schematic diagram of the experimental setup for oscillating pressure patch clamp flexoelectric measurements of direct flexoeffect in native membranes. Membrane patch curvature oscillations were excited by a loudspeaker-driven system fed by a function generator (Model 126, Exact Electronics). Static pressure variations were produced by a reversible peristaltic pump. Pressure (P_0) was monitored by a pressure meter bridge based on a MPX100AP silicon piezoresistive pressure sensor. The membrane current (I) was amplified by a patch clamp amplifier (EPC 7, List Electronics) and then passed to a dual lock-in amplifier (SR530, Stanford Research Systems). Membrane current (I) and voltage (Vhold), flexo (I_f) and pressure (P) outputs were recorded on a four-channel analog tape recorder (RACAL). In some cases just two of these signals were digitally recorded by a two-channel PCM (Sony) linked to a standard videorecorder (from [7], with permission from the publisher).

The first experimental demonstration of the flexoelectric response of locust muscle membranes was done in 1989 [72]. Already at that time strong interference from channel activity of membrane patches was observed, therefore a channel-free patch may be an advantage for such measurements. Apart from the application of oscillating pressure, the preparation and patching procedure closely followed the standard protocols. Patches in either cell-attached, inside-out, or outside-out configurations were studied. Tip diameters could not exceed 1 μm, though, because with larger tips giga-seal formation was precluded.

The data illustrated in Fig. 10 [74] were obtained with an inside-out patch oscillating in the high frequency range (150–500 Hz). Oscillation frequencies were selected at which the standing waves of sound pressure were maximal at the pipette holder end of the plastic tube. Keeping the pressure amplitude constant, a linear increment of the first harmonic amplitude of 30 fA(rms)/Hz was observed. An extrapolation of the amplitude–frequency relationship passed through zero, very similar to the BLM situation. Thus, this observation represents the capacitance component of the flexocurrent (Eq. 26). In that case, estimating the curvature radius as equal to the tip radius, i.e. 0.7 μm (with an error allowance of 50%), we can calculate a flexocoefficient of 2.5×10^{-18} C for locust muscle membrane, a quite substantial value.

9.7. *Atomic force microscopy (AFM) and converse flexoeffect of native membranes*

Electrically stimulated membrane motions in cells were investigated first using AFM [78]. The experimental setup and some results are shown in Fig. 11. Voltage-clamped HEK293 cell membranes under ±10 mV peak–peak AC carrier stimulus with an AFM cantilever pressed against the membrane moved the tip some nm normal to the plane of the membrane. These movements tracked the voltage at frequencies >1 kHz with a phase lead of 60–120°, as expected of a displacement current. Tip displacement

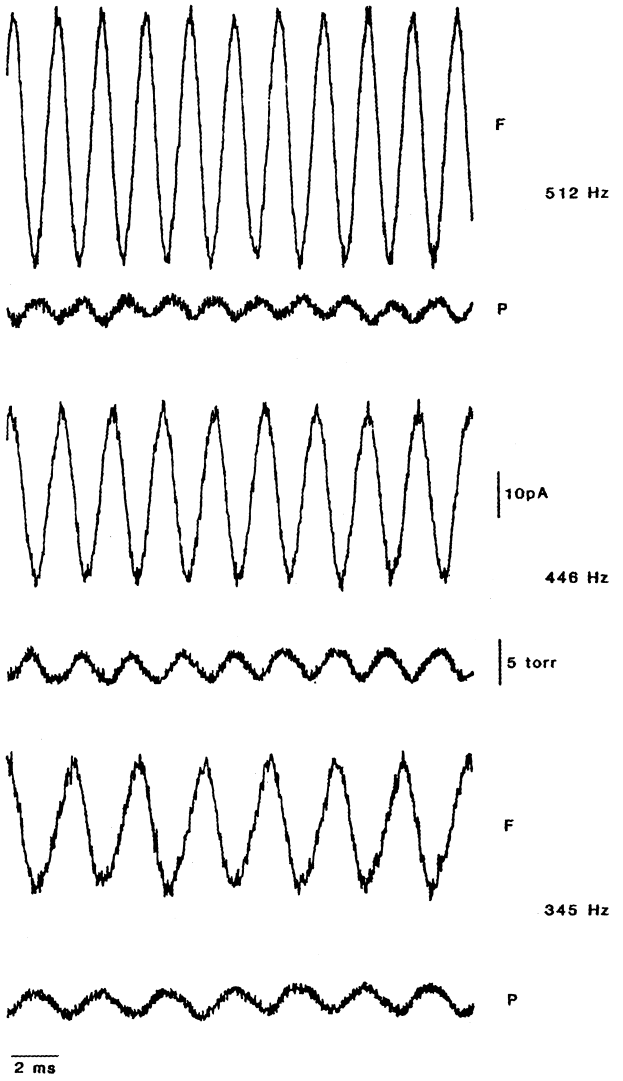

Fig. 10. Flexoelectric recordings from an inside-out patch excised from locust muscle membrane in standard locust saline. Pipette resistance was 6.7 MΩ. Seal resistance was 0.5 GΩ. Patch capacitance components were $C_{fast} = 7.5$ pF and $C_{slow} = 0.8$ pF. Upper traces: flexoelectric response (F) of the patch at three different frequencies (345 Hz, 446 Hz and 512 Hz) in the high frequency range. Lower traces: driving pressure signals (P). Current bar of 10 pA and pressure bar of 5 torr apply to all measurements. Flexoelectric signals were strong enough to be directly recorded from the List amplifier output. No voltage dependence of the first harmonic was observed (i.e. patch oscillated around its flat state). At 345 Hz, with 2.4 torr(pp) driving pressure a first harmonic flexoresponse of 9 pA(rms), phase −72° was observed. The control pick-up response after rupturing the patch and taking the pipette tip out of the saline was much lower (0.23 pA) and had a completely different phase (170°) (from [7], with permission from the publisher).

(at a cantilever stiffness of 0.01 N/m) was roughly about 0.1 nm/mV and outward with depolarization, meaning a positive sign of flexocoefficient. From the estimations made in [78] one can infer a value of 10^{-19} C for the flexocoefficient of the HEK293 membrane. This value is lower than the locust muscle one, which is not surprising in view of the marked mechanoelectric behaviour of the muscle membrane.

Further experimental results using pulsed excitation were recently obtained [79]. Rectangular pulses of 60 ms duration and linearly increasing amplitude produced membrane displacements in linear proportion to the voltage pulse amplitude. Hyperpolarizing the membrane increased the local curvature around the tip moving it inward, i.e. a positive sign of the flexocoefficient is confirmed at normal ionic strength. However, a sign reversal was found at lower ionic strengths of the bath, below 10 mM.

10. Summary of the results

The experimental results reported so far are summarized in Table 1. All data in this table refer to the high frequency range of curvature oscillations, above 200–300 Hz, i.e. to the blocked flexocoefficient f^B.

To make comments on the consistency of data, we should refer to Sections 5 and 6. The pure dipolar contribution, order of magnitude 1×10^{-20} C, is observed only in the case of fully synthetic GMO and DPhPC (5 and 8), with strictly zero surface charge. Still, the values are a few times higher than the theory predicts. Also, within the experimental errors they are practically equal, although DPhPC has two ester group dipoles, while GMO has only one and the surface potentials of lecithin membranes are some 200 mV higher than those of GMO [80]. This difference may be related to the very different radii of BLM of GMO and patch membranes of DPhPC (two orders of magnitude).

In all other cases the charge contribution predominates, as already mentioned. Moreover, only the shift of surface charge equilibrium under the global electric neutrality conditions can explain the observed values, of the order of magnitude 1×10^{-18} C. The difference in signs between PE and PC flexocoefficients, 1 and 2, is puzzling and needs further attention. The PE sign corresponds to the global

Table 1
Flexoelectric coefficients of BLMs (1–7) and membrane patches (8 and 9) made from different lipids under various ionic conditions

Lipid; electrolyte	Partial charge per lipid head β (%)	Flexocoefficient ($\times 10^{-19}$ C)	Ref.
(1) Phosphatidylethanolamine from *E. coli*; 50 mM KCl	−3.7%	−25.5 (±72.5%)	[37]
(2) Phosphatidylcholine from egg yolk; 0.1 M NaCl	−0.4%	+26.5 (±50%)	[62], recalculated
(3) Phosphatidylcholine from egg yolk; 0.1 M NaCl+1 mM UO_2^{2+}	approx. 100%	−120 (±10%)	[62], recalculated
(4) Phosphatidylcholine from egg yolk; 0.1 M KCl	−18.8%	13 (±0.2%)	[58], recalculated
(5) Glyceryl mono-oleate (synthetic); 0.1 M KCl	0	0.43 (±0.5%)	[58], recalculated
(6) Phosphatidylserine from bovine brain; 0.1 M KCl	approx. −100%	20 (±25%)	[38], recalculated
(7) Phosphatidylserine from bovine brain; 0.1 M KCl+1 mM UO_2^{2+}	approx. 100%	151 (±19%)	[68], converse flexoeffect, fitted data
(8) Diphytanoylphosphatidylcholine (synth.); 0.15 M KCl	0	0.31 (±29%)	[77], patch clamp
(9) Locust muscle membrane; standard locust saline	>100%	25 (±50%)	[74], patch clamp

1–3, and 8 and 9, electrical estimation of curvature; 4–7, interferometric measurement of curvature, sign determination of f not attempted. All experiments except 7 concern the direct flexoeffect. All data refer to the high frequency range above 200–300 Hz, i.e. to the blocked flexocoefficient f^B.

electric neutrality case, Eq. 19. The PC sign might imply a detailed electric neutrality; however, in such a case it should have been much lower, cf. Eq. 16.

The equality between direct and converse flexocoefficients of UA-modified membranes (3 and 7) demonstrates the validity of the Maxwell relation, as we noted before.

11. Photoflexoelectricity

Black lipid membranes modified with semiconductor nano-sized CdS particles ('nanomembranes') serve as models of photosensitive native cell membranes, where CdS crystallites mimic membrane proteins [81]. Nanomembranes are known to display photoelectric effects. Like some biomembranes, they are capable of transformation of the optical energy into an electrical one.

Periodic variations of membrane curvature with such membranes lead to the discovery of a new effect, named 'photoflexoelectricity' [82].

The formation and development of CdS nanocrystalline particulate films on the GMO BLM surface were followed by optical microscopy. Significant changes in both the amplitude and phase of the flexoresponse were found between the light and dark state of the membrane. The increase in the flexoelectric response accompanying illumination, referred to as photoflexoelectricity, was followed by a return to the initial dark value when the light was switched off. For a given GMO BLM, this photoflexoelectric response was reproducible for many cycles. The curvature-induced membrane potential (Fig. 12) measured under zero current clamp (open external circuit) showed a reversible increase of its amplitude following light–dark cycles. Photokinetic curves of the flexoelectric voltage were fitted with single exponentials demonstrating a faster rise after illumination ($\tau^L = 13$ s) and a slower decay to the dark level ($\tau^D = 20$ s).

The flexoelectric amplitude increments and the phase shifts caused by illumination of BLMs with increasing amount of particles generated on the membrane were studied [82]. The dark response decreased as the amount of CdS particles increased (as judged from the visual appearance), but the difference (light–dark) became more and more pronounced. At the same time, a tendency towards larger phase shift at higher photoflexoelectric response was observed. The frequency dependence of the effect was found to be nearly linear in both the light and the dark state.

A mechanism of photoflexoelectricity in nanomembranes was proposed and compared to the experiment.

The first observation of photoflexoelectricity in such a system permits to speculate upon the possible existence of this phenomenon in native membranes as well. The existence of a converse effect (i.e. photo-

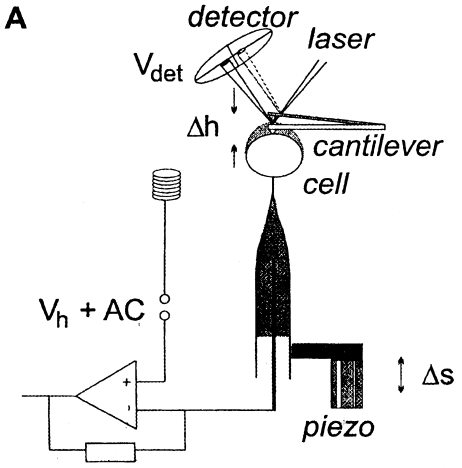

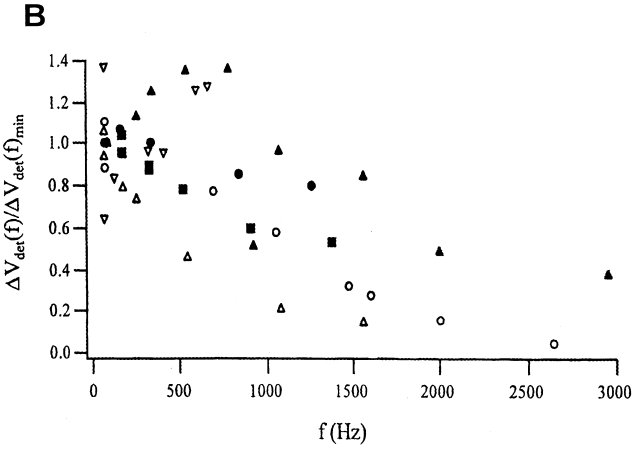

Fig. 11. (A) Scheme of the experimental setup for combined patch clamp–AFM measurements of converse flexoeffect in native membranes. The patch pipette holding the HEK cell was attached to the tubular piezo ceramic used for x, y, z scanning. The holding potential V_h and the AC carrier voltage were applied to the cell by the patch clamp amplifier (EPC 7). The cantilever movement was translated into a voltage, V_{det}, by the laser and quadrant detector. The output was proportional to the height difference Δh of the surface. (B) Frequency dependence of the voltage-induced membrane movements of six HEK cells normalized to the amplitude of the lowest frequency tested. In three experiments a stiffer cantilever with $k = 0.02$ N/m was used (normal cantilever, $k = 0.01$ N/m). The mean sensitivity at the lowest frequency was (0.15 ± 0.05) nm/mV$_{pp}$ (mean ± S.E.M., $n = 6$). The decrease of signal amplitude at higher frequencies is affected by the detection system (resonance frequency 2 kHz) (reproduced from the Journal of General Physiology 111 (1998) 65–74 [78], by copyright permission of the authors and the Rockefeller University Press).

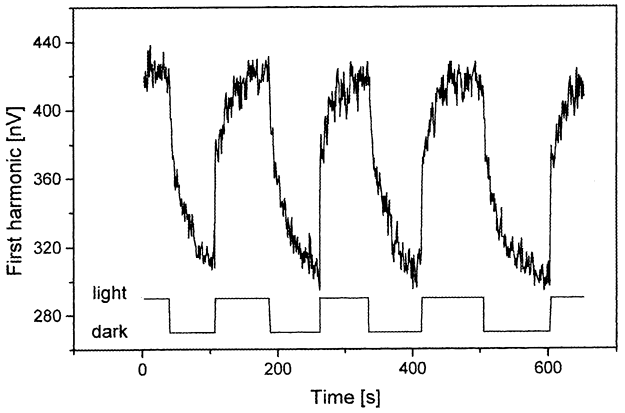

Fig. 12. Flexoelectric response of a GMO BLM coated with CdS nanoparticles, oscillating at 700 Hz under zero current clamp. The first harmonic of the membrane potential is measured. The increase of the flexoelectric signal after UV light flashing shows exponential rise kinetics and reversible decay (from [7], with permission from the publisher).

potential-induced membrane curvature upon illumination) also seems highly probable. The connectivity between the membrane shape (curvature), the light intensity and the membrane potential could be related to the mechanism responsible for the phototaxis and other photoadaptive phenomena on the cell membrane level.

These findings could also stimulate the development of photo-mechano-electric sensors and actuators for molecular electronics.

12. Implications of flexoelectricity

In a physical system with three degrees of freedom (mechanical, electrical and optical) the possible energy interconversion effects, involving two or three degrees of freedom simultaneously, can be classified in the following way. *Two degrees of freedom*: (1) mechano-electric effect (direct) and (2) electro-mechanic effect (converse); (3) opto-electric effect (direct) and (4) electro-optic effect (converse); (5) mechano-optic effect (direct) and (6) opto-mechanic effect (converse). *Three degrees of freedom*: (7) mechano-electro-optic effect; (8) mechano-opto-electric effect; (9) electro-mechano-optic effect; (10) electro-opto-mechanic effect; (11) opto-mechano-electric effect; (12) opto-electro-mechanic effect.

The total number of effects thus amounts to at

least 12, because in the case of three degrees of freedom additional subclasses are possible with respect to input/output combinations. At present, just a few of them are experimentally demonstrated in membrane systems, as follows.

Effects 1 and 2 are the flexoelectric effects discussed above, direct and converse ones. Flexoelectricity [83] is a fundamental property of liquid crystals, relating their mechanical and electrical degrees of freedom. As we have seen above, in membranes (living and model) flexoelectricity provides a linear relationship between membrane curvature and membrane polarization (Effect 1), or transmembrane voltage and membrane bending stress (Effect 2). It is closely related to mechanosensitivity and mechanotransduction, basic features of living systems [75].

Earlier, a model using direct flexoelectric effect for transformation of mechanical into electrical energy in the hearing process in stereocilia was proposed [75] (Fig. 13). Recently, the converse flexoeffect that transforms mechanical into electrical energy was employed for description of the electromotility of outer hair cell membrane (Fig. 14) [84]. Electromotility plays a central role in the process of mechanoamplification, which is vital for the hearing of high frequency sounds [94,95].

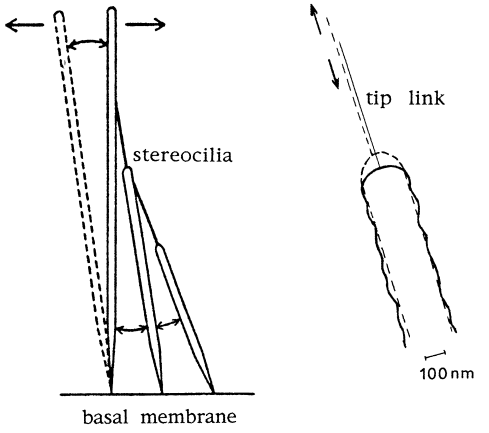

Fig. 13. A model for applying stress to the membranes of stereocilia in hair cells. The left panel shows how tilting of the bundle of cilia to the left (excitatory excursion) leads to stretching of the membranes because of the pull by the tip links. This first observation explains the modulation in the stress sensitive channel functioning. The right panel shows that the tip curvature under excitatory/inhibitory tilt is increased/decreased. This second observation permits us to speculate on a flexoelectric sensing mechanism (from [7], with permission from the publisher).

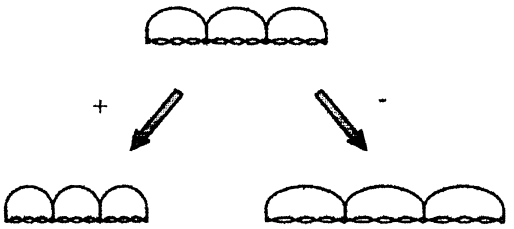

Fig. 14. Micromechanical model for outer hair cell converse flexoeffect. Curvature changes in the elemental motile unit cause extension of the spectrin molecules attached to the pillar proteins. Three units are shown in the figure. A membrane depolarization (+) leads to a decrease in the radius of curvature and a shortening of the cell while hyperpolarization (−) leads to an increase of the radius of curvature and cell lengthening (from [84], with permission from the authors and the publisher).

The understanding of the mechanism(s) of membrane mechanosensitivity would open the way for the construction of artificial bioelectronic mechanosensors and actuators with mechanical input and electrical output or vice versa. Exchange of sound waves on the cellular and subcellular level could then be open for research.

Many other important membrane functions are connected with the creation of membrane curvature at a certain stage (e.g. endocytosis, virus budding, cell and organelle morphogenesis, cell movement by pseudopodia, and cell contact). The out-of-plane fluctuations of membranes (e.g. the flicker phenomenon in erythrocytes) provide a typical example of fluctuating membrane curvature. It could bring about an attractive flexoelectric force at short distances, relevant to the cell–cell contact [85]. In all these phenomena curvature-induced polarization is by no means present, and the acknowledgement of the consequences of its presence can be of crucial importance for deeper understanding of what happens [7]. Participation of flexoelectricity in passive and active membrane ion transport was postulated [10,12] and recently corroborated [86,7]. Therefore, the prospect of flexoelectricity as an intricate relationship between membrane mechanics and membrane electrodynamics is rather high.

A third, optical degree of freedom of membrane systems was recently explored in a flexoelectric context. In an opto-mechano-electric membrane system the number of possible combinations between its

three degrees of freedom (serving either as inputs or outputs) is greatly increased. Moreover, due to the ultimate existence of these degrees of freedom in some native membranes, new hints about the structure–function relationship in photosynthetic membranes, retinal rods and discs, and other photoactive membranes could be obtained.

Effect 3 is known as the photoelectric effect, i.e. a photo-induced charge separation across nanomembranes giving rise to photocurrent or photovoltage [87,88]. This effect has also been named the 'chemical capacitance effect' [89]. Effect 4 would be demonstrated as electroluminescence of a membrane, i.e. light generation by transmembrane voltage. This effect has been observed in native photosynthetic membranes [90].

Effect 11 (and, in fact, also Effect 8) is the photoflexoelectricity phenomenon discussed above. Both optical and mechanical degrees of freedom acting as inputs, the electric degree served as output. The rest of the combined three-degrees' effects has not been demonstrated yet, and represents a promising field for future studies.

A further, chemical degree of freedom was not specially discussed here, but it is clear that it is inherent to all others, at least because all coupling coefficients (elastic, flexoelectric, dielectric, photoelectric, etc.) are functions of membrane chemistry [7]. The same considerations are valid for the thermal degree of freedom.

A very important feature of a membrane system having two or more degrees of freedom should be pointed out: the possibility of occurrence of deterministic chaos in it [91]. According to the Bendixon–Poincaré theorem, a dynamic system can be chaotic in a three-dimensional or higher-dimensional phase space. Each degree of freedom provides one generalized coordinate and one generalized force. Therefore, even a simple flexoelectric membrane (four-dimensional phase space) does possess all the necessary features for the arising of dissipative, self-organizing structures. These might have played an important role at the level of prebiotic evolution of matter [91,92].

Finally, by establishing the general principles of functioning of membrane mechanisms, membranologists will be prepared to proceed with the preparation of examples of 'protocells' (or membrane machines [93]), based on giant vesicular membrane structures with several degrees of freedom, as above.

13. Conclusion

We have extended Schrödinger's postulate [1] for the cell membranes. We underlined the role of a specific mechanical degree of freedom, membrane curvature, in that respect. We stressed the importance of the flexoelectricity phenomenon in the interrelation of the mechanical degree of freedom with the electrical, optical, and chemical degrees of freedom of membranes. This really makes the remarkable analogy of Schrödinger between a cell and a clock mechanism [1] richer, as the 'membrane clock' is now regarded not simply a mechanical one, but, for example, electro-mechano-optical (just like a liquid crystal wristwatch), thermo-chemi-mechanical, etc. Flexoelectric concepts reviewed here could also be of primary importance in the construction of artificial membrane machines ('protocells'), as well as electromechanical sensors and actuators for molecular electronics.

Acknowledgements

The author is indebted to Dr. I. Bivas and Prof. F. Sachs for constructive reading of the manuscript.

References

[1] E. Schrödinger, What is Life? Edinburgh Univ. Press, Edinburgh, 1943.
[2] G.H. Brown, J.J. Wolken, Liquid Crystals and Biological Structures, Academic Press, New York, 1979.
[3] P. Bothorel, C. Lussan, C.R. Hebd. Seances Acad. Sci. 266C (1968) 2492–2496.
[4] S.J. Singer, G.L. Nicolson, Science 175 (1972) 720–731.
[5] S.J. Singer, J. Membr. Biol. 129 (1992) 3–12.
[6] W. Helfrich, Z. Naturforsch. 28c (1973) 693–703.
[7] A.G. Petrov, The Lyotropic States of Matter: Molecular Physics and Living Matter Physics, Gordon and Breach Publ., New York, 1999.
[8] R.B. Meyer, Phys. Rev. Lett. 22 (1969) 918–924.
[9] W.P. Mason, Piezoelectric Crystals and their Application to Ultrasonics, D. van Nostrand, New York, 1950.

[10] A.G. Petrov, in: Physical and Chemical Bases of Biological Information Transfer, Plenum Press, New York, 1975, pp. 111–125.
[11] A.G. Petrov, A. Derzhanski, J. Phys. 37 (Suppl.) (1976) C3–C155.
[12] A.G. Petrov, S.A. Seleznev, A. Derzhanski, Acta Phys. Pol. A55 (1979) 385.
[13] A.G. Petrov, Nuovo Cimento 3D (1984) 174–192.
[14] A. Derzhanski, Phys. Lett. 139A (1989) 170–173.
[15] D.A. Pink, M. Belaya, V. Levadny, B. Quinn, Langmuir 13 (1997) 701–1711.
[16] R.H. Pearson, I. Pasher, Nature 281 (1979) 499–501.
[17] R.F. Flewelling, W.L. Hubbell, Biophys. J. 49 (1986) 541–552.
[18] K. Gawrisch, D. Ruston, J. Zimmerberg, V.A. Parsegian, R.P. Rand, N. Fuller, Biophys. J. 61 (1992) 1213–1223.
[19] J.T. Davies, E.K. Rideal, Interfacial Phenomena, Academic Press, New York, 1963.
[20] S.J. Marrink, M. Berkowitz, H.J.C. Berendsen, Langmuir 9 (1993) 3122–3131.
[21] E. Egberts, S.J. Marrink, H.J.C. Berendsen, Eur. Biophys. J. 22 (1994) 423–436.
[22] K.V. Damodaran, K.M. Merz Jr., Langmuir 9 (1993) 1179–1183.
[23] K.V. Damodaran, K.M. Merz Jr., Biophys. J. 66 (1994) 1076–1087.
[24] M.A. Wilson, A. Pohorille, J. Am. Chem. Soc. 116 (1994) 1490–1501.
[25] F. Zhou, K. Schulten, J. Phys. Chem. 99 (1995) 2194–2207.
[26] K. Gawrisch, V.A. Parsegian, D.A. Hajduk, M.W. Tate, S.M. Gruner, N.L. Fuller, R.P. Rand, Biochemistry 31 (1992) 2856–2864.
[27] J.N. Israelachvili, Intermolecular and Surface Forces, 2nd edn., Academic Press, London, 1992.
[28] I. Bivas, M. Kozlov, Liquid Crystals 8 (1990) 813–817.
[29] H. Morgan, D.M. Taylor, O.N. Oliveira Jr., Biochim. Biophys. Acta 1062 (1991) 149–156.
[30] F. Vilallonga, Biochim. Biophys. Acta 163 (1968) 290–300.
[31] H. Bürner, M. Winterhalter, R. Benz, J. Colloid Interface Sci. 168 (1994) 183–189.
[32] M.M. Standish, B.A. Pethica, Trans. Faraday Soc. 64 (1968) 1113–1120.
[33] A. Cavalli, O.N. Oliveira Jr., Rev. Sci. Instrum. 66 (1995) 5567–5569.
[34] K. Hristova, I. Bivas, A.G. Petrov, A. Derzhanski, Mol. Cryst. Liq. Cryst. 200 (1991) 71–77.
[35] K. Hristova, I. Bivas, A. Derzhanski, Mol. Cryst. Liq. Cryst. 215 (1992) 237–244.
[36] M. Winterhalter, W. Helfrich, J. Phys. Chem. 96 (1992) 327–330.
[37] A.G. Petrov, V.S. Sokolov, Eur. Biophys. J. 13 (1986) 139–155.
[38] A. Todorov, A.G. Petrov, J.H. Fendler, Langmuir 10 (1994) 2344–2350.
[39] A.G. Petrov, I. Bivas, in: S.G. Davison (Ed.), Progress in Surface Science, Vol. 16, Pergamon Press, New York, 1984, pp. 389–512.
[40] R. Mutafchieva, PhD Thesis, Bulg. Acad. Sciences, Sofia, 1985.
[41] P. Schlecht, Biopolymers 8 (1969) 757–767.
[42] W. Ortung, Biochemistry 9 (1970) 2394–2410.
[43] D.M. Hayes, P.A. Kollman, J. Am. Chem. Soc. 98 (1976) 3335–3345.
[44] H. Gruler, E. Sackmann, Croat. Chem. Acta 49 (1977) 379–386.
[45] V.S. Markin, Biofizika 25 (1980) 941–952.
[46] R. Henderson, Annu. Rev. Biophys. Bioeng. 6 (1977) 87–120.
[47] J.B. Robinson, D.S. Parsons (Eds.), Biological Membranes, Clarendon Press, Oxford, 1975.
[48] D.E. Green, S. Ji, R.F. Brucker, Bioenergetics 44 (1972) 527–570.
[49] C.R. Hackenbrock, J. Cell Biol. 30 (1967) 269–297.
[50] C.R. Hackenbrock, J. Cell Biol. 37 (1968) 345–369.
[51] R.A. Harris, J.T. Penniston, J. Asai, D.E. Green, Proc. Natl. Acad. Sci. USA 59 (1968) 830–840.
[52] D.E. Green, J.A. Young, Am. Sci. 59 (1971) 92–97.
[53] A.L. Lehninger, Biochemistry. The Molecular Basis of Cell Structure and Function, Worth Publ., New York, 1972.
[54] A. Zhivkov, PhD Thesis, Bulg. Acad. Sci., Sofia, 1995.
[55] V.I. Passechnik, V.S. Sokolov, Biofizika 18 (1973) 655–660.
[56] A.L. Ochs, R.M. Burton, Biophys. J. 14 (1974) 473–489.
[57] A. Derzhanski, A.G. Petrov, Y.V. Pavloff, J. Phys. Lett. 42 (1981) L119–L122.
[58] A.T. Todorov, A.G. Petrov, M.O. Brandt, J.H. Fendler, Langmuir 7 (1991) 3127–3137.
[59] S. Stoylov, Colloid Electro-optics; Theory, Techniques and Applications, Academic Press, London, 1991.
[60] P. Mueller, D.O. Rudin, H. Ti Tien, W.C. Wescott, Nature 194 (1962) 979–980.
[61] K. Sun, J. Phys. Chem. 101 (1997) 6327–6330.
[62] A. Derzhanski, A.G. Petrov, A. Todorov, K. Hristova, Liquid Crystals 7 (1990) 439–449.
[63] S.G.A. McLaughlin, G. Szabo, G. Eisenman, J. Gen. Physiol. 58 (1971) 667–680.
[64] S.I. Sukharev, L.V. Chernomordik, I.G. Abidor, Yu.A. Chizmadzhev, Elektrokhimiya 17 (1981) 1638–1650.
[65] A. Todorov, PhD Thesis, Syracuse University, 1993.
[66] O. Alvarez, R. Latorre, Biophys. J. 21 (1978) 1–10.
[67] X.K. Zhao, S. Baral, R. Rolandi, J.H. Fendler, J. Am. Chem. Soc. 110 (1988) 1012–1020.
[68] A. Todorov, A.G. Petrov, J.H. Fendler, J. Phys. Chem. 98 (1994) 3076–3079.
[69] B. Sakmann, E. Neher, B. Sakmann, E. Neher (Eds.), Single Channel Recording, Plenum Press, New York, 1983, pp. 37–52.
[70] R. Coronado, R. Latorre, Biophys. J. 43 (1983) 231–236.
[71] T. Schürholz, H. Schindler, FEBS Lett. 152 (1983) 187–190.
[72] A.G. Petrov, R.L. Ramsey, P.N.R. Usherwood, Eur. Biophys. J. 17 (1989) 13–17.

[73] A.G. Petrov, P.N.R. Usherwood, B.A. Miller, Mol. Cryst. Liq. Cryst. 215 (1992) 109–119.
[74] A.G. Petrov, B.A. Miller, K. Hristova, P.N.R. Usherwood, Eur. Biophys. J. 22 (1993) 289–300.
[75] A.G. Petrov, P.N.R. Usherwood, Eur. Biophys. J. 23 (1994) 1–19.
[76] M. Sokabe, F. Sachs, Z. Jing, Biophys. J. 59 (1991) 722–728.
[77] N.I. Hristova, Master Thesis, St. Kliment Ochridski Univ., Sofia, 1994.
[78] J. Mosbacher, M. Langer, J.K.H. Horber, F. Sachs, J. Gen. Physiol. 111 (1998) 65–74.
[79] P.-Ch. Zhang, A.M. Keleshian, F. Sachs, Nature, submitted.
[80] O.S. Andersen, G. Giebisch, D.C. Tosteson, H.H. Ussing (Eds.), Membrane Transport in Biology. Concepts and Models, Vol. 1, Springer Verlag, Heidelberg, 1978, pp. 369–446.
[81] J.H. Fendler, Membrane-Mimetic Approach to Advanced Materials, Springer-Verlag, Berlin, 1994.
[82] M. Spassova, A.G. Petrov, J.H. Fendler, J. Phys. Chem. 99 (1995) 9485.
[83] P.G. de Gennes, J. Prost, The Physics of Liquid Crystals, 2nd edn., Clarendon Press, Oxford, 1993.
[84] R.M. Raphael, A.S. Popel, W.E. Brownell, Biophys. J. 78 (2000) 2844–2862.
[85] I. Bivas, A.G. Petrov, J. Theor. Biol. 88 (1981) 459–483.
[86] A.G. Petrov, Cell. Mol. Biol. Lett. 2 (Suppl. 1) (1997) 231–253.
[87] S. Baral, J.H. Fendler, J. Am. Chem. Soc. 111 (1989) 1604–1610.
[88] X.K. Zhao, S. Baral, R. Rolandi, J.H. Fendler, J. Am. Chem. Soc. 110 (1988) 1012–1018.
[89] D. Mauzerall, H. Gerischer, J.J. Katz (Eds.), Light-Induced Charge Separation in Biology and Chemistry, Dahlem Konferenzen, Berlin, 1979, p. 241.
[90] V. Brumfeld, I.R. Miller, R. Korenstein, Biophys. J. 56 (1989) 607–614.
[91] M. Bushev, Synergetics: Chaos, Order, Self-Organization, World Scientific, Singapore, 1994.
[92] S.A. Seleznev, L.M. Fedorov, A.I. Michailov, A.M. Borisova, S.I. Kusina, Zh. Evol. Khim. Fiziol. 12 (1976) 411–416.
[93] R. Lipowsky, in: Statistical Mechanics of Biocomplexity, Lecture Notes in Physics, Springer, Berlin, 1999, p. 527.
[94] V.I. Passechnik, Mekhanizmi ulitki organa slukha, Accounts Sci. Techn. VINITI, Moscow, Hum. Anim. Physiol. Ser. 39 (1988) 6–121.
[95] W.E. Brownell, A.A. Spector, R.M. Raphael, A.S. Popel, Annu. Rev. Biomed. Eng. 3 (2001) in press.